IN-34

314 646

NASA

MEMORANDUM

STRUCTURE OF WEAK SHOCK WAVES

IN A MONATOMIC GAS

By L. Talbot and F. S. Sherman

University of California

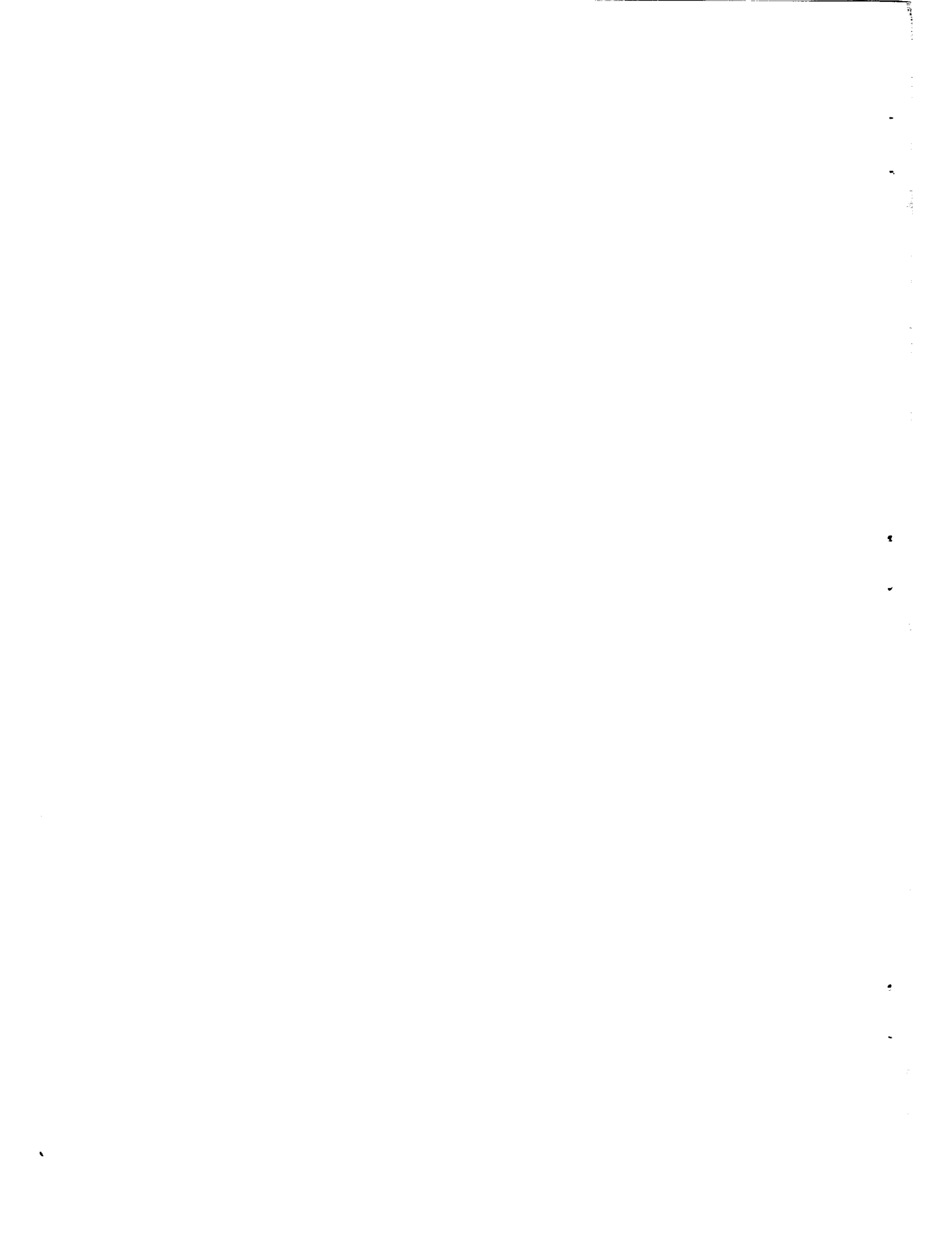# NATIONAL AERONAUTICS AND SPACE ADMINISTRATION

WASHINGTON

January 1959

NATIONAL AERONAUTICS AND SPACE ADMINISTRATION

MEMORANDUM 12-14-58W

STRUCTURE OF WEAK SHOCK WAVES

IN A MONATOMIC GAS

By L. Talbot and F. S. Sherman

SUMMARY

The profiles and thicknesses of normal shock waves in argon at Mach numbers of 1.335, 1.454, 1.576, and 1.713 were determined experimentally by means of a free-molecule probe whose equilibrium temperature is related by kinetic theory to the local flow properties and their gradients.

Comparisons were made between the experimental shock profiles and the theoretical profiles calculated from the Navier-Stokes equations, the Grad 13-moment equations, and the Burnett equations. New, very accurate numerical integrations of the Burnett equations were obtained for this purpose with results quite different from those found by Zoller, to whom the solution of this problem is frequently attributed.

The experimental shock profiles were predicted with approximately equal success by the Navier-Stokes and Burnett theories, while the 13-moment method was definitely less satisfactory. A surprising feature of the theoretical results is the relatively small difference in predictions between the Navier-Stokes and Burnett theories in the present range of shock strengths and the contrastingly large difference between predictions of Burnett and the 13-moment theories. It is concluded that the Navier-Stokes equations are correct for weak shocks and that within the present shock strength range the Burnett equations make no improvement which merits the trouble of solving them. For shocks of noticeably greater strength, say with a shock Mach number of more than 2.5, it remains fundamentally doubtful that any of these theories can be correct.

INTRODUCTION

A new experimental method for measuring shock-wave structure involving the use of a free-molecule probe was introduced by Sherman in reference 1. He made his measurements in a low-density wind tunnel, where the shock waves produced were thick enough to permit local measurements within them while the probe, being small compared with the mean free path, did not disturb the macroscopic flow pattern. This technique enabled him to

obtain information on the shape and thickness of the shock profiles which could be compared in a detailed fashion with the predictions of several theories for shock structure.

The free-molecule probe used by Sherman was essentially a cylindrical wire whose temperature could be measured. The wire was stretched across the jet of the wind tunnel and was mounted on a mechanism which traversed it through the normal shock waves formed at the open end of a hollow conical shock holder. The data obtained consisted of point-by-point profiles giving the variation of wire equilibrium temperature with position through the shock waves.

Experimental wire-temperature profiles were compared with predictions based on the Navier-Stokes equations, the Grad 13-moment equations, and a kinetic-theory method of Mott-Smith. The Burnett equations were not used by Sherman because of the difficulty in solving them for the shock-wave boundary-value problem.

Sherman's experimental data were much better predicted by the Navier-Stokes equations than by the more complex kinetic-theory methods. However, the comparison among the various theories was somewhat clouded by two facts: (1) Most of the experimental data was obtained for diatomic gases, whereas the kinetic theory has been fully developed only for monatomic gases, and (2) the shocks tested were too strong, falling outside the range of Mach numbers for which a single-valued shock-transition solution of the 13-moment equations exists.

In an attempt to remove the two objections listed above, the measuring technique of reference 1 was applied to shock waves in argon at Mach numbers of 1.335, 1.454, 1.576, and 1.713. On the basis of the experimental accuracy obtained by Sherman and the magnitude and character of the differences in predictions between the Navier-Stokes and 13-moment theories, it was hoped that these new experiments would be capable of discriminating clearly between the competing theories. The present report describes the new measurements and rounds out the comparison with theory by including high-speed computing-machine solutions of the Burnett equations.

SYMBOLS

a	Zoller's shock-strength parameter
b,c	coefficients in equation (A5)
$\vec{C}$	dimensionless peculiar molecular velocity
E	specific internal energy, cm^2/sec^2
f	molecular velocity-distribution function
H_0, H_1, H_2, H_3	Bell-Schaaf speed-ratio functions
h_c	convective heat-transfer coefficient for free-molecule flow
$I_0(s^2/2)$	modified Bessel function of first kind, order zero, and argument $s^2/2$
$I_1(s^2/2)$	modified Bessel function of first kind, order one, and argument $s^2/2$
i	electric current, amp
i,j	indexes, used as subscript $(i,j = 1,2,3)$
K	thermal conductivity of wire, ergs/cm sec $^{\circ}K$
k	thermal conductivity of gas, ergs/cm sec $^{\circ}K$
L_*	reference length, $\mu_*/\rho u$
L_1	reference length, $\mu_1/\rho u$ (used in table I)
l	half length of wire
M_1	shock Mach number
m	mass flow constant, equations (B3), gm/cm^2 sec
n	number density of gas molecules, cm^{-3}
P	momentum constant, equations (B3), $dynes/cm^2$
p	thermodynamic pressure, $dynes/cm^2$
p_i	impact pressure, $dynes/cm^2$

p_{ij}	components of viscous-stress tensor, e.g., p_{xx}, p_{yy}, p_{zz}, dynes/cm^2
P_{xx}, P_{yy}, P_{zz}	components of excess viscous-pressure tensor, dynes/cm^2
p_{xx}'	Navier-Stokes part of p_{xx}, dynes/cm^2
p_{xx}''	Burnett part of p_{xx}, dynes/cm^2
p_o	reservoir stagnation pressure, dynes/cm^2
Q	energy constant, equations (B3), ergs/cm^2 sec
q_i	heat-flux vector component, e.g., q_x, ergs/cm^2 sec
q_x	heat flux, ergs/cm^2 sec
q_x'	Navier-Stokes part of q_x
q_x''	Burnett part of q_x
R	gas constant for argon, ergs/cm ^{o}K
R'	resistance of wire per unit length, ohms/cm
$(R')_o$	resistance of wire at temperature T_o, ohms
$(R')_w$	resistance of wire at temperature T_w, ohms
R_1, R_2	functions defined in equations (B11)
r	radius of wire, cm
$s = u/\sqrt{2RT}$	molecular speed ratio
$t = \dfrac{T_w}{T_o} - 1$	
$t_{aw} = \dfrac{T_{aw}}{T_o} - 1$	

T	gas temperature, ^{O}K
T_{aw}	adiabatic wire equilibrium temperature, ^{O}K
T_{O}	stagnation (room) temperature, ^{O}K
T_{w}	wire equilibrium temperature
T_{*}	reference temperature, ^{O}K, $\dfrac{2}{\gamma + 1} T_{O}$
u	gas velocity, cm/sec
$\vec{u}$	mean flow velocity, cm/sec
v	dimensionless velocity, equations (B8)
v_{ν}	boundary value of v
w	normalized, dimensionless velocity, equations (B18)
x	distance along flow, cm
y	Grad's dimensionless distance, equation (1)
z	Zoller's dimensionless distance, equations (B8)
α	thermal accommodation coefficient of wire
α_{T}	temperature coefficient of resistance, $^{O}K^{-1}$
γ	specific-heats ratio
$\delta_{m}^{(u)}(x), \delta_{m}^{(u)}(y)$	maximum-slope shock-wave thickness, based on velocity profile and measured in units of x and y, respectively
$\delta_{m}(T_{w})$	maximum-slope shock-wave thickness based on wire-temperature profile
ϵ	Grad's shock-strength parameter, equation (2)
ϵ_{O}	radiant emissivity of wire at temperature T_{O}

ϵ_w radiant emissivity of wire at temperature T_w

η' dimensionless Navier-Stokes stress, equations (B8)

η'' dimensionless Burnett stress, equations (B8)

$\bar{\eta}$ initial stress perturbation amplitude, equations (B14)

ϑ temperature perturbation, equations (B13)

$\bar{\vartheta}$ initial temperature perturbation amplitude, equations (B14)

θ_i Burnett heat-flux coefficients

$\Lambda_1 = \dfrac{16}{5}\sqrt{\dfrac{5}{6\pi}}\dfrac{M_1\mu_1}{\rho u}$ Maxwellian mean free path ahead of shock, cm

λ root of characteristic equation (B16)

μ viscosity, poises

μ_* viscosity at reference temperature T_*, poises

μ_1 viscosity ahead of shock, poises

ν boundary value index, equations (B12)

$\vec{\xi}$ absolute molecular velocity, cm/sec

ξ_i ith component of $\vec{\xi}$

ξ' dimensionless Navier-Stokes heat flux, equations (B8)

ξ'' dimensionless Burnett heat flux, equations (B8)

$\bar{\xi}$ initial heat-flux perturbation amplitude, equations (B14)

ρ gas density, gm/cm^3

σ Stephan-Boltzmann constant, $ergs/cm^2$ sec $^\circ K$

τ dimensionless temperature variable, equations (B8)

τ_ν boundary value of τ

Ω velocity perturbation, equations (B13)

$\bar{\Omega}$	initial velocity perturbation amplitude, equations (B14)
ω	exponent of viscosity-temperature law
ω_i	Burnett stress coefficients, used in appendix B

EXPERIMENTAL APPARATUS

Mach 1.5 Nozzle

The experiments were performed in the open-jet, continuous-flow, low-density wind tunnel at the University of California, Berkeley. This wind tunnel is described in reference 2. For the purposes of the present experiments a nozzle was designed and built to give an exit Mach number of 1.5 in a monatomic gas at design flow conditions. This proved to be an extraordinary supersonic nozzle. Evidently, because the combination of low exit Mach number and extremely thick nozzle boundary layers, the nozzle is not subject to the formation of oblique shocks or sharp rarefaction fans at the exit lip when the pressure in the test chamber is raised or lowered from the exit static pressure of the open jet. What appears to happen instead is that a rise in test-chamber pressure at any given stagnation-chamber pressure only produces a smooth increase in boundary-layer thickness along the entire nozzle length. This in turn yields an effective nozzle of smaller bore and area ratio than the original but of equal contour smoothness. Lowering the chamber pressure just reverses the effect. The outcome of this behavior is a great flexibility of selection of Mach and Reynolds numbers, obtained by independent adjustment of stagnation-chamber and test-chamber pressures, without sacrifice of flow uniformity. This was exploited in the present experiments by making all shock-wave surveys at approximately the same free-stream mean-free-path length. The four shocks were then of roughly equal thickness and could be surveyed with correspondingly equal accuracy. The nozzle exit diameter was 7.91 inches, and the diameter of the isentropic core of flow varied from 3 to 4 inches over the range of Mach numbers covered here. Impact pressure surveys taken at the exit plane are shown in figure 1.

Nozzle Calibration

Because of the extreme importance of an accurate determination of Mach number for the present tests, the method of nozzle calibration was very critical. Several different independent methods for determining the Mach number were used, and the worth of the final calibration is shown by the excellent agreement obtained among these methods.

The instruments used were a 0.300-inch-diameter source-shaped impact probe, corrected for viscous effects by the methods of reference 3, and a 0.300-inch-diameter static-pressure probe. The latter had 8 pressure orifices equally spaced around its periphery at a cross section 13 inches from the 10° conical tip and 13 inches upstream from the cross-stream support. When the pressure orifices were positioned in the test region, the tip of the probe protruded into the stagnation chamber so that tip effect was avoided. The 13-inch length downstream of the pressure orifices permitted the probe to be traversed throughout the axial length of the nozzle and minimized cross-stream support interferences. The static probe was assumed to be free of viscous effects. Its diameter was small compared with the nozzle throat diameter of approximately 6 inches. No change in nozzle wall pressure was observed upon insertion or removal of the probe, and excellent agreement was found between wall pressure and probe pressure under conditions where the probe surveys indicated constant static pressure across the jet.

The two local pressure measurements, impact p_i and static p, were combined to determine the local Mach number from the ratio p_i/p. In addition, the Mach number was determined from the ratios p_i/p_0 and p/p_0, where p_0 is the stagnation pressure, assuming an isentropic flow.

As a final check on the internal consistency of the Mach numbers determined in the above fashion, the free-stream equilibrium temperature of the free-molecule probe used for the shock-wave surveys was measured. Although the probe was initially uncalibrated, in that its radiation losses were unknown but significant, the probe was extremely sensitive to Mach number variation in the Mach number range of the tests. A smooth correlation between probe equilibrium temperatures and Mach numbers determined from pressure measurements was essential for confidence in the latter.

The final calibrated flow conditions used in the tests are listed in table I. The Mach number values, cited to three decimal places, represent averages of the values obtained from the several methods. Individual values differed from these averages by less than 1 percent.

Shock Holder

A single shock holder, similar in design to those employed in the tests of reference 1, was used throughout the present experiments. It is shown in figure 2. The entry diameter was 3 inches, which is about the dimension of the isentropic core of the nozzle flow at the lowest Mach number $M_1 = 1.335$ (see fig. 1). The shock holder was slotted to provide for motion of the wire probe downstream of the entry plane, but

this provision turned out to be unnecessary since all the shock waves used in the tests were slightly detached. An internal included angle of divergence of 40° was selected for the shock holder, which represented a compromise between the estimated minimum internal angle required to allow for boundary-layer growth within the shock holder and the maximum external angle for an attached shock wave. These two conditions could not be met simultaneously at the low Mach numbers of the tests, and therefore the shock waves were slightly detached. However, the glow photographs of the shock-holder operation (fig. 3) indicate that at least the central portions of the shock waves were plane. The shock-detachment distance decreased with increasing Mach number.

Free-Molecule-Flow Equilibrium-Temperature Probe

The 0.00025-inch-diameter tungsten resistance-wire probe described in reference 1 was used for all the shock-wave measurements. A schematic diagram of the resistance-wire instrument is shown in figure 4. In every case the Knudsen number of the probe (the ratio of the mean free path in the gas to the probe diameter) was greater than 50, which insured that free-molecule-flow conditions always prevailed.

The wire resistance was found to vary linearly with temperature over the temperature range encountered in the tests. An oven calibration gave

$$(R')_W = (R')_O \left[1 + \alpha_T(T_W - T_O)\right]$$

with $(R')_O$ equal to about 30 ohms at 23° C (the exact value differing from probe to probe, depending on the length of the measuring section) and $\alpha_T = 0.00332$ per °C, also at 23° C.

The wire current of 0.100 ± 0.001 milliampere was supplied by a 1.34-volt mercury cell in series with dropping resistances and was measured by observation of the potential drop across a 30.0-ohm resistance. This potential drop and also that across the measuring section of the free-molecule probe were measured with a Rubicon hand-balancing potentiometer and a Leeds and Northrup galvanometer. The combined potentiometer-galvanometer system had a resolution of better than 1 microvolt (0.1 microvolt could be estimated), which is about 0.5 percent of the probe potential change between upstream and downstream limits of the weakest shock wave tested. Alinement of the free-molecule wire parallel to the plane of the shock-holder entry was accomplished by adjusting the wire supporting frame and by bending the heavier "tails" of the wire leads. The alinement was checked before and after the tests, and it was estimated that the maximum misalinement error was not greater than about 0.003 inch over the length spanned by the measuring section. If it is assumed that this misalinement

only causes the wire to read the average signal of a perfectly alined wire over a 0.0015-inch-travel through the shock, one can demonstrate graphically that this produces no significant change in the measured shock profile.

Wire-Traversing Arrangement

The wire setup, shown in figure 2, is essentially the same as the system described in reference 1. The wire was moved by a small electric motor; its position was indicated by a 1-inch-travel, 0.0001-inch-reading Ames dial indicator.

Flow Visualization

Unfortunately, an extremely bright afterglow in argon was discovered only after the program was completed and, consequently, did not contribute to the exploratory phases of the experiments. However, pictures were obtained with it (fig. 3) which confirmed, a posteriori, certain important conclusions about shock placement and shape which had been formed from observation of wire-temperature traces.

Gas Supply

The argon used for the tests was supplied by Linde Air Products Co. and was guaranteed to be 99.9 percent pure. It was introduced directly into the wind tunnel without additional drying or purification. Some air leaks into the wind tunnel, of course, and may mix with the argon in small amounts. What one fears is the presence of an impurity of a molecular weight very different from that of the test gas in sufficient amount to add diffusion to the dissipative mechanisms broadening the shock. It can be shown theoretically (e.g., ref. 4) that 1 percent of air in argon, a very liberal allowance for possible leakage, produces less than 1/2 percent shock thickening by diffusion.

EXPERIMENTAL RESULTS

Free-Stream Probe Readings and Radiation Corrections

Initial measurements were made with the free-molecule probe in the uniform stream at the Mach numbers chosen for the final shock-wave test. These data are shown in figure 5. The wire-temperature readings fell consistently below the theoretical values given by the analysis of reference 5. On examining the possible reasons for the discrepancy it was found that the losses due to heat conduction were small but that a sizable

loss might be expected from radiative heat transfer. An acceptable fit to all the free-stream data was obtained with a value of $\epsilon_O/\alpha = 0.13$ where ϵ_O is the emissivity of the wire at room temperature and α is the thermal accommodation coefficient of argon on tungsten (see appendix A).

The existing experimental arrangement did not permit accurate independent determinations of the quantities ϵ_O and α. However, the correlation between free-stream Mach number and probe temperature, using the single value $\epsilon_O/\alpha = 0.13$, was sufficiently good to warrant acceptance of this value as an accurate calibration constant for the probe.

It should be noted that the formula for free-molecule-flow convective heat transfer given by equation (A2) of reference 1 is in error. The correct formula is given by equation (A3) of this paper.

Shock-Wave Profiles

The principal results of the experiments are shown by the data points plotted in figures 6(a) to 6(d). In these figures the ratio of the measured wire temperature T_w to the measured stagnation temperature T_O is plotted against the nondimensional space variable y. This nondimensional length is related to the physical distance x of the shock-wave traverse by

$$y = \frac{4}{35} \frac{\epsilon x}{L_*} \tag{1}$$

in which ϵ is the shock strength introduced by Grad (ref. 6) and is defined in terms of the initial Mach number M_1 by

$$\epsilon = \frac{15\left(M_1^2 - 1\right)}{3 + 5M_1^2} \tag{2}$$

and L_* is a reference length pertaining to the value μ_* of the viscosity at the temperature $T_* = \frac{2}{\gamma + 1} T_O = \frac{3}{4} T_O$. It is defined by

$$L_* = \frac{\mu_*}{\rho u} \tag{3}$$

The value $T_* = \dfrac{2}{\gamma + 1} T_O$ corresponds to the value of the gas temperature at the sonic point of an adiabatic flow having total temperature T_O.

The major difference between the method used here to present the data and that employed in reference 1 is that in this report the data have not been "normalized" so as to make the downstream end points of the shock wave agree with theory. The normalization technique used in reference 1 is open to some criticism; although it does not alter the maximum-slope thicknesses of the shock waves, it obscures some features of the data.

THEORETICAL CALCULATIONS

The theoretical procedures for finding shock-wave profiles in terms of the temperature of a free-molecule wire with no radiation or metallic conduction losses are given in detail in reference 1 for the Navier-Stokes and 13-moment equations. Extensions of these procedures to correct the predicted profiles for radiation losses and to include use of the Burnett equations are given in appendixes A and B of the present report. The following paragraphs will review, for convenience, only the basic philosophy of the theoretical approach.

The computation of free-molecule-flow energy transfer to the wire requires knowledge of the distribution of molecular velocities at the wire location. Thus, the initial object of the analysis is to find the molecular distribution function f at each point within the shock wave. For the calculations discussed here f is assumed in the form of a local Maxwellian distribution skewed by the viscous stress and heat flux; that is,

$$f(\vec{\xi},x) = \frac{n}{(2\pi RT)^{3/2}} e^{-C^2} \left[1 + \frac{p_{ij}}{p} C_i C_j + \frac{q_i C_i}{p\sqrt{2RT}} \left(\frac{2}{5} c^2 - 1 \right) \right] \qquad (4)$$

In this C is the peculiar molecular velocity $\Big($absolute velocity $\vec{\xi}$ minus mean flow velocity $\vec{u}\Big)$ divided by $\sqrt{2RT}$. All the parameters $\Big(n,$ $u,$ $p,$ $T,$ $p_{ij},$ and $q_i\Big)$ are functions of x.

If this distribution function is substituted into the Boltzmann equation and the moments of that equation taken with respect to 1, ξ_i, and $\frac{1}{2}\xi_i\xi_i$, one obtains the familiar conservation equations of fluid mechanics. These equations initially form an indeterminate set because of the explicit appearance of the stress- and heat-flux variables. The problem at hand is then threefold: (1) The conservation equations must be supplemented to yield a determinate set, (2) this set must be solved

for the shock-wave boundary-value problem, thus determining n, u, and so forth as functions of x, and (3) the distribution function, now known as a function of x, must be applied to calculate the wire-temperature shock profile.

The three theories used here differ, for the immediate purpose, only in the way they supplement the conservation equations to find a determinate set. Two basic kinetic-theory methods are involved, these being the Chapman-Enskog method and the Grad method. The Chapman-Enskog method yields first the Navier-Stokes and then the Burnett expressions for viscous stress and heat flux, as successive approximations in a series expansion in the mean free path. The coefficients of this series involve only n, u, T, and their spatial derivatives (ref. 7). The Grad method relates p_{ij} and q_i to n, u, p, and T by taking higher order moments of the Boltzmann equation. This introduces further unknown variables, and the heart of the Grad method is the choice of some physically sound way to truncate the procedure. The truncation which corresponds to the simple distribution function (4) yields the 13-moment equations, in which p_{ij} and q_i appear explicitly (ref. 8).

The differential equations to be solved for the shock-wave structure are thus the Navier-Stokes equations, Burnett equations, and 13-moment equations. Previous authors, notably Grad (ref. 6), Gilbarg and Paolucci (ref. 9), and Zoller (ref. 10) have indicated how these equations may be integrated numerically, and their methods were applied quite directly.

Once the distribution function is determined throughout the shock, it is used to compute the wire temperature according to the procedures of Bell and Schaaf (ref. 11).[1] For the present range of shock strengths it is sufficient to use the approximate form of their result

$$\frac{T_{aw}}{T} = H_0(s) + H_1(s)\frac{p_{xx}}{p} + H_2(s)\frac{p_{yy}}{p} + H_3(s)\frac{q_x}{pu} \tag{5}$$

---

[1]This method makes use of the Grad distribution function, in which p_{ij} and q_i enter as parameters. The Grad distribution function is valid for both the 13-moment and Navier-Stokes equations. However, the Burnett distribution function contains higher order terms in the peculiar molecular velocity C, which possibly makes a significant contribution to the wire temperature, but to the authors' knowledge, the explicit form of the complete Burnett distribution function has never been worked out. The procedure employed in this report was to calculate Burnett wire-temperature profiles using the Grad distribution function, with values of p_{ij} and q_i obtained from the Burnett shock-wave solutions. No quantitative estimate of the error involved in this procedure is available at the present writing.

for a wire lying along the z-axis with flow in the x-direction. In this equation, the $H_i(s)$ are functions of the molecular speed ratio, $s = u/\sqrt{2RT}$, as given in reference 11. For a one-dimensional flow of a monatomic gas the Stokes relation

$$p_{xx} + p_{yy} + p_{zz} = 0 \tag{6}$$

is valid, as is the equation

$$p_{yy} = p_{zz} = -\frac{1}{2}p_{xx}$$

regardless of the particular form employed for p_{xx} when the flow is in the x direction.

Finally, since radiation heat losses were obviously important in these experiements, the theoretical curves were corrected for these losses by the method of appendix A. It is interesting to observe that the radiation losses cause a decrease in maximum shock slope, as seen in the wire-temperature profile, but cause virtually no change in measured shock thickness.

The recent kinetic theory of Ikenberry and Truesdell (refs. 12 and 13) has not been used in this report but is currently being applied to the shock-wave problem by others. Mott-Smith's theory, used in reference 1, was judged too unsuccessful in that work to be employed again here.

The particular calculations which were made are listed below.

(1) Navier-Stokes theory: T_w/T_o profiles were calculated for $M_1 = 1.335, 1.454, 1.576,$ and 1.713 by numerical integration, using the viscosity-temperature law given in reference 14. These profiles are shown in figures 6(a) to 6(d), respectively. The velocity profile at $M_1 = 1.576$ is shown in figure 7(a); here w is the nondimensional velocity defined in equations (B18).

(2) 13-moment theory: Wire-temperature profiles were calculated for Maxwellian molecules at $M_1 = 1.335$ and 1.576. These are shown in figures 6(a) and 6(c), respectively. Velocity profiles for $M_1 = 1.576$ and 1.713 are shown in figures 7(a) and 7(b), respectively. The 13-moment profiles become double-valued for $M_1 > 1.65$.

(3) Burnett theory: Wire-temperature profiles were calculated for Maxwellian molecules at $M_1 = 1.342, 1.454, 1.576,$ and 1.732. These are shown in figures 6(a), 6(b), 6(c), and 6(d), respectively. The velocity profiles for $M_1 = 1.576$ and 1.732 are shown in figures 7(a) and 7(b), respectively.

(4) Effect of viscosity-temperature law on theoretical profiles: In addition to the calculations listed above, a Navier-Stokes profile for Maxwellian molecules was calculated for $M_1 = 1.713$, and a 13-moment profile for the empirical viscosity law $\mu = \mu(T)$ was calculated at $M_1 = 1.576$. These profiles were compared respectively, with the Navier-Stokes $\mu(T)$ profile at $M_1 = 1.713$ and the 13-moment Maxwellian molecule profile at $M_1 = 1.576$. When these profiles are drawn with y or x/L_* as the dimensionless distance variable, the maximum slope is virtually independent of the viscosity-versus-temperature law (the point at which $T = T_*$ is usually very close to the point of maximum slope). The Maxwellian molecule profiles are slightly steeper upstream of the maximum-slope point, and more gradual downstream, than are the $\mu = \mu(T)$ profiles. However, the differences are too slight in the present Mach number range to be seen in figures 6(c) and 6(d). Had x/Λ_1, with Λ_1 the mean free path upstream of the shock, been used as abscissa, a noticeable difference between these profiles would be seen. Then the Maxwellian molecule profile would be the thickest of the family obtained from the viscosity laws $\mu \propto T^\omega$ $(0 \leqq \omega \leqq 1)$.

DISCUSSION

Agreement Between Data and Downstream

Rankine-Hugoniot Conditions

It is seen from figures 6(a) to 6(d) that, except in the case of the $M_1 = 1.713$ shock wave, the downstream end points indicated by the data are considerably higher than the theoretical curves. Higher values of T_w/T_0 correspond to higher Mach numbers, and the data indicate that the pressure rise through the shock waves was not so great as that predicted by theory. These discrepancies are probably due to the influence of the shock holder. In all the shock waves tested a region of reacceleration followed the leveling-off region of the subsonic tail. Apparently the lower pressures in the accelerating subsonic flow within the shock holder propagate upstream into the subsonic tail of the shock wave, broadening and weakening it. The effect is less pronounced for stronger shock waves, as evidenced by the better agreement found here at higher Mach numbers and also by comparison with Sherman's helium data. (The effect mentioned above was found, to a lesser extent, also in Sherman's tests but it is not so apparent in the normalized profiles.)

Comparisons With Various Theories

Of the theoretical curves shown in figures 6(a) to 6(d), those found from the Navier-Stokes equations seem to fit the data best, particularly

in the upstream half of the shock wave. There is, however, little choice
between this fit and that afforded by the Burnett equations; indeed the
latter equations seem slightly more successful in the downstream half of
the shock. This last fact is not too significant, because of the previ-
ously mentioned possibility that the downstream tail of the shock may be
distorted to an unknown degree by the failure to produce experimentally
the proper downstream boundary condition. The 13-moment equations give
a definitely inferior fit to these profiles.

The rather close coincidence of the Navier-Stokes and Burnett pre-
dictions came as a surprise to the present authors, largely because a
casual reading of Zoller's paper (ref. 10) had left the impression that
he had already integrated the Burnett equations, finding results consid-
erably closer to those of the 13-moment method than to those of the
Navier-Stokes method. In fact, Zoller's basic equations do not arise
from the Chapman-Enskog method, and while they are quite similar to the
Burnett equations (as given in up-to-date form in ref. 15) they are
evidently significantly different when applied to the shock-wave prob-
lem. Mrs. Chang's calculations with the correct Burnett equations
(ref. 16) failed to warn of this fact because of their poor convergence.
On the other hand, Grad reexpanded her results and gave, in a note "added
in proof" to reference 6, approximate formulas which predicted that the
relative shock-wave thicknesses according to the three theories consid-
ered here would be just about as we have found them numerically.

Various authors have suggested that an approximate solution by
series-expansion techniques is most appropriate to the Navier-Stokes,
Burnett or 13-moment equations, since these equations are themselves
derived by series methods applied to the Boltzmann equation. Good
examples of this method are found in references 16 and 17.

As was done by Wang Chang (ref. 16) a series solution was con-
structed for the shock-wave problem, for the Burnett equations, and for
the "third approximation" equations which contain, in addition to the
Burnett terms, the linear third-derivative terms which arise from the
next Chapman-Enskog approximation. The expansion technique was that
suggested by Grad (ref. 6, p. 284) carried to order ϵ^2, at which stage
the first contributions of the third approximation appear. These cal-
culations verified Grad's formulas for the shock-wave thicknesses
(ref. 6, p. 300) and provided the associated shock profiles. While the
series solution of the Burnett equations, carried only to this degree
in ϵ, did not agree closely with the computing-machine solutions, it
is believed that the series results predict the correct qualitative
effect (a further thickening of the shock) of the third-derivative terms.
The point which appears significant is that successive approximations in
the Chapman-Enskog scheme seem to move the theoretical predictions far-
ther from, rather than closer to, the experimental data. In this connec-
tion it is interesting to recall that the Burnett equations can be

obtained by iteration on the 13-moment equations (ref. 18, p. 258). If in this sense the Burnett equations are regarded as approximations to the 13-moment equations, the fact that the 13-moment equations predict thicker shock waves than the Burnett equations is consistent with the aforementioned effect of higher-order approximations in the Chapman-Enskog scheme.

There seems to be no satisfactory explanation of the observation that presumably more accurate solutions of the Boltzmann equation fail to yield increasingly accurate predictions of the experimental data. The following possibilities can be suggested: (1) The Boltzmann equation is correct, but existing series methods of solving it are very slowly convergent or perhaps only asymptotic; (2) the series solutions are adequately convergent, but the Boltzmann equation itself is inapplicable in shock waves of moderate strength; or (3) both the Boltzmann equation and these methods of solution are wrong for this problem. At least, a clear indication that distribution functions of the form given in equation (4) are not correct for all shock strengths is exhibited in reference 19. There these functions are shown to become negative in certain ranges of molecular velocity for shock waves only slightly stronger than those investigated here. This is an obvious violation of the definition of a distribution function.

Maximum-Slope Thickness

Most investigators of shock-wave structure have used the Prandtl maximum-slope velocity thickness as a means for comparing the results of different calculations. In units of y, this velocity thickness is defined by

$$\delta_m^{(u)}(y) = \frac{u_2 - u_1}{\left(\dfrac{du}{dy}\right)_{max}} \tag{7}$$

or, in units of x,

$$\delta_m^{(u)}(x) = \frac{35L_*}{4\epsilon} \delta_m^{(u)}(y) \tag{8}$$

This is, of course, only one of several maximum-slope thicknesses that can be constructed. For instance, temperature or density thicknesses can be determined from the shock-wave solution, and from the experiments performed here wire-temperature thicknesses can be obtained. Most of

the theoretical shock-wave analyses have been presented in terms of velocity thickness; therefore it will be advantageous to represent the wire-temperature maximum-slope-thickness data in terms of equivalent velocity thicknesses.

It may be remarked that a maximum-slope thickness (of any of the quantities, velocity, temperature, etc.) is not a particularly good measure of the prediction of a given theory, since it depends on a purely local property of the shock wave. Conceivably, two different theories could predict similar maximum-slope thicknesses yet give profiles which were markedly different in shape. Both Grad (ref. 6) and Gilbarg and Paolucci (ref. 9) have remarked on this, and Grad introduced an "area thickness" which reflects better the overall shape of the profile than does the maximum-slope thickness. However, the area thickness is a rather awkward quantity to use, so the maximum-slope thickness has been employed here.

The experimental wire-temperature thicknesses $\left[\delta_m^{(T_w)}\right]_{exp}$, obtained by drawing a maximum-slope line through the data, were transposed to experimental velocity thicknesses through the correspondence

$$\left[\frac{\delta_m^{(T_w)}}{\delta_m^{(u)}}\right]_{theor} = \left[\frac{\delta_m^{(T_w)}}{\delta_m^{(u)}}\right]_{exp} \tag{9}$$

This ratio ran from 1 to about 1.07 as M_1 increased from 1.34 to 1.73, according to the Burnett theory, for which the most detailed profiles were calculated. Maximum-slope shock thicknesses transposed in this fashion are shown in figures 8 and 9 and tabulated in table I. In the figures they show ranges of ±5-percent error, which are felt to give a fair estimate of the accuracy with which the experimental maximum slope could be found.

Comparison With Other Experimental Data

There still appears to be just one other source of experimental data on shock thicknesses, the work of Hornig and his colleagues at Brown University (currently being continued at Princeton). This utilizes the optical reflectivity technique, in which light of a wave length chosen nearly equal to the anticipated shock thickness is intercepted obliquely by a shock traveling down a tube. Given a theoretical density profile, and hence an index-of-refraction profile for the shock

wave, one can compute its reflectivity for light of a given wave length and angle of incidence. The theoretical result is mostly sensitive to the ratio of shock thickness to light wave length and comparatively insensitive to the detailed shape of the density profile. Hence if a reasonable profile shape may be assumed, the calculation may be performed with the shock thickness carried along as a scale factor, to be determined empirically by matching predicted and observed reflectivities. This work, including some recent and refined data on shock thicknesses in argon, has been summarized by Hornig in reference 20. Results shown in figures 8 and 9 agree remarkably well with the present data, considering the completely different experiments. Unfortunately, the data in reference 20 attributed to Talbot and Sherman contained a small calculation error when supplied to Dr. Hornig. The fact that Hornig's data and the present results agree better in figure 9 than in figure 8 is not an accident.

The viscosity of argon is very poorly represented by $\mu \propto T^{\omega}$ (ω = Constant) over any considerable temperature range. In the present investigation wind-tunnel data $T_* \approx$ Constant = 225° K, and $\omega \approx 0.9$, while in Hornig's data, $T_1 \approx$ Constant = 300° K, and $\omega \approx 0.8$. Figure 8 gives the truer comparison of these two sets of data since δ_m/L_* is virtually independent of moderate changes in the viscosity-temperature law.

CONCLUDING REMARKS

The profiles and thicknesses of normal shock waves in argon at Mach numbers of 1.335, 1.454, 1.576, and 1.713 were determined experimentally by means of a free-molecule probe whose equilibrium temperature is related by kinetic theory to the local flow properties and their gradients.

Comparisons were made between the experimental shock profiles and the theoretical profiles calculated from the Navier-Stokes equations, the Grad 13-moment equations, and the Burnett equations. New, very accurate, numerical integrations of the Burnett equations were obtained for this purpose, with results quite different from those found by Zoller, to whom the solution of this problem is frequently attributed.

The experimental shock profiles were predicted with approximately equal success by the Navier-Stokes and Burnett theories, while the 13-moment method was definitely less satisfactory. A surprising feature of the theoretical results is the relatively small difference in predictions from Navier-Stokes and Burnett theories in the present range of shock strengths and the contrastingly large difference between predictions of the Burnett and Grad theories. It is concluded that the Navier-Stokes equations are correct for weak shocks and that within the

20

present shock-strength range the Burnett equations make no improvement
which justifies the trouble of solving them. For shocks of substantially
greater strength, it remains fundamentally doubtful that any of these
theories can be correct.

University of California,
    Berkeley, Calif., January 1, 1958.

APPENDIX A

FREE-MOLECULE-PROBE HEAT LOSSES

Radiation-Convection Heat Balance

Consider first a probe in a uniform stream. The probe has an equilibrium temperature T_w which is less than the adiabatic equilibrium temperature T_{aw}. Heat is transferred to the probe by convection and is lost from the probe by radiation. (For the time being, conduction losses and i^2R heating will be neglected.)

A heat balance for the probe is, per unit length,

$$2h_c \pi r \alpha (T_{aw} - T_w) = 2\pi r \sigma \left(\epsilon_w T_w{}^4 - \epsilon_o T_o{}^4 \right) \tag{A1}$$

in which ϵ_w is the emissivity of the wire at temperature T_w and ϵ_o is its emissivity at the surrounding temperature T_o. For a pure metal, $\epsilon_w/\epsilon_o = T_w/T_o$ (ref. 21), so

$$h_c \alpha (T_{aw} - T_w) = \sigma \epsilon_o T_o{}^4 \left[\left(\frac{T_w}{T_o} \right)^5 - 1 \right] \tag{A2}$$

If this equation is used to correlate the free-stream equilibrium-temperature data, with

$$h_c = \frac{\rho u \mathrm{Re}^{-s^2/2}}{\sqrt{\pi} s} \left[(1 + s^2) I_0 \left(\frac{s^2}{2} \right) + s^2 I_1 \left(\frac{s^2}{2} \right) \right] \tag{A3}$$

then it is found that the single value $\epsilon_o/\alpha = 0.13$ gives a curve for T_w/T_o which passes through all of the data points, as shown in figure 5. In this figure, the T_{aw}/T_o curve was calculated from the functions given in reference 5.

The value $\epsilon_o/\alpha = 0.13$ seems to be rather large. A typical value for the emissive power of tungsten at room temperature is $\epsilon_o = 0.03$, and values cited in reference 22 for the accommodation coefficient of argon on tungsten range from $\alpha = 0.53$ (clean tungsten) to $\alpha = 1.0$

(surface saturated with argon). However, it is not clear whether the above values apply for the situation at hand. For example, there was undoubtedly a layer of adsorbed air on the wire, and also the surface condition of the wire, which affects both ϵ_0 and α, was unknown. In addition, the wire geometry itself was rather complicated, since it was constructed with two copper-plated lap joints at the potential lead junctions, and these double-strand joints make up almost 20 percent of the measuring span. Because of these aforementioned uncertainties, it seems most reasonable to accept the value $\epsilon_0/\alpha = 0.15$ simply as a calibration constant and to refrain from more specific interpretation.

Estimate of Conduction End Losses

The full heat balance for the wire, including conduction and current heating but neglecting changes in resistance and conductivity with temperature, is

$$\frac{d^2 T_w}{dx^2} - \frac{2\sigma\epsilon_0 T_0^4}{Kr}\left[\left(\frac{T_w}{T_0}\right)^5 - 1\right] + \frac{2h_c\alpha}{Kr}(T_{aw} - T_w) + \frac{i^2 R'}{\pi Kr^2} = 0 \qquad (A4)$$

The boundary conditions at $x = 0$ are, with $x = 0$ taken at the center of the wire span,

$$\frac{dT_w}{dx} = 0$$

and, at $x = \pm l$,

$$T = T_0$$

Putting

$$T_w = T_0(1 + t)$$

$$T_{aw} = T_0(1 + t_{aw})$$

equation (A4) may be linearized and solved, with the result

$$t = \frac{b}{c^2}\left(1 - \frac{\cosh cx}{\cosh c\ell}\right) \tag{A5}$$

where

$$b = \frac{2h_c \alpha t_{aw}}{Kr} - \frac{i^2 R'}{\pi Kr^2 T_o}$$

$$c = \frac{10\sigma\epsilon_o T_o^3}{Kr} + \frac{2h_c \alpha}{Kr}$$

For a numerical example, consider the conditions which were obtained at $M_1 = 1.713$ in the free stream. Take

$\sigma = 5.6733 \times 10^{-5}$ ergs/cm^2 $^\circ$K sec

$K = 2 \times 10^7$ ergs/cm $^\circ$K sec

$r = 3.17 \times 10^{-4}$ cm

$T_o = 296.5^\circ$ K

$i = 1 \times 10^{-4}$ amp

$R' \approx 15$ ohms/cm

$\alpha_T = 0.00332/^\circ$K

$h_c = 1.51 \times 10^4$ ergs/cm^2 $^\circ$K sec

$\epsilon_o/\alpha = 0.13$

$\alpha = 1.0$

$T_{aw}/T_o = 1.221$

$t_{aw} = 0.221$

Then, $c = 2.25$ cm^{-1} and $\frac{b}{c^2} = 0.2075$. It is found also that the effects of i^2R' heating are negligible. The most difficult thing to estimate is the effective half length l between the wire center and the assumed end-point heat sink at temperature T_0. In the actual tests the current and potential leads spanned about 19 centimeters. However, only about 10 centimeters of this span was immersed in the uniform stream, the remaining $4\frac{1}{2}$ centimeters on each end being in the nozzle boundary layer and outside the jet. It is known also that the equilibrium temperature of the wire within the boundary layer is actually higher than it is in the uniform flow, so there is in fact some heat input to the wire in these regions. Since only an estimate of the conduction effect is needed, the rather pessimistic choice $cl = 10$ is made. Then,

$$t \approx 0.2075\left(1 - \frac{\cosh 2.25x}{11,000}\right) \tag{A6}$$

The measuring span of the wire was about 2 centimeters, so with $x = 1$,

$$(t)_{x=1} \approx 0.2070 \tag{A7}$$

Even if the conduction losses are doubled to account for heat flow out the potential leads, it is evident that these losses are still negligible, since the difference between the center-point temperature and the temperature at $x = 1$ is, from equation (A7),

$$(T_w)_{x=0} - (T_w)_{x=1} \approx 0.001(T_{aw} - T_0) \approx 0.065° \text{ C}$$

Note that the center point temperature ratio with correction for radiation obtained from this linearized calculation is

$$\left(\frac{T_w}{T_0}\right)_{x=0} = 1.2075$$

which is quite close to the exact value obtained from equation (A2) for the flow conditions chosen.

Radiation Corrections to Theoretical Shock Profile

For comparison with the experimental results, the calculated T_{aw}/T_0 profiles were corrected, point by point, for radiative heat losses. The heat-transfer coefficient which is appropriate to a nonuniform flow was taken from reference 11 and is

$$h_c = \frac{\rho u Re^{-s^2/2}}{\sqrt{\pi}s}\left\{(1 + s^2)I_0\left(\frac{s^2}{2}\right) + s^2I_1\left(\frac{s^2}{2}\right) + \frac{P_{xx}}{4p}\left[I_0\left(\frac{s^2}{2}\right) - I_1\left(\frac{s^2}{2}\right)\right] + \right.$$

$$\left. \frac{P_{yy}}{4p}\left[I_0\left(\frac{s^2}{2}\right) + I_1\left(\frac{s^2}{2}\right)\right] - \frac{q_x}{5pu}\left[sI_0\left(\frac{s^2}{2}\right) - sI_1\left(\frac{s^2}{2}\right)\right]\right\} \qquad (A8)$$

This heat-transfer coefficient and the value $\epsilon_0/\alpha = 0.13$ were employed with equation (A2) to obtain the corrected profiles.

APPENDIX B

INTEGRATION OF BURNETT EQUATIONS

The Burnett equations for one-dimensional flow are nearly identical to those integrated for a shock wave by Zoller in 1951. Zoller's method of integration is so thoroughly presented in reference 10 that it was quite simple to set up the Burnett equations for the solutions described here by merely copying his procedures. This was done, as follows.

The three conservation equations for one-dimensional steady flow of a fluid are

$$
\left.
\begin{aligned}
&\frac{d}{dx}(\rho u) = 0 \\[2mm]
&\frac{d}{dx}(\rho u^2 + p + p_{xx}) = 0 \\[2mm]
&\frac{d}{dx}\left[\rho u\left(E + \frac{1}{2}u^2\right) + u(p + p_{xx}) + q_x\right] = 0
\end{aligned}
\right\} \tag{B1}
$$

in which ρ is the mass density, u, the flow velocity, p, the pressure, E, the internal energy, q_x, the x component of heat flux, and p_{xx}, the x component of excess viscous pressure. For a perfect monatomic gas,

$$
\left.
\begin{aligned}
E &= \frac{3}{2}RT \\[2mm]
p &= \rho RT
\end{aligned}
\right\} \tag{B2}
$$

The differential system of equations (B1) may be integrated once to yield

$$
\left.
\begin{aligned}
\rho u &= m \\
\rho u^2 + p + p_{xx} &= P \\
\rho u^3 + 5pu + 2p_{xx}u + 2q_x &= Q
\end{aligned}
\right\} \tag{B3}
$$

where P, Q, and m are constants of the flow.

The viscous stress p_{xx} may be expressed as

$$p_{xx} = p_{xx}' + p_{xx}'' \tag{B4}$$

with $p_{xx}' = -\dfrac{4}{3}\mu\dfrac{du}{dx}$, the familiar Navier-Stokes expression. Similarly, the heat flux q_x may be written

$$q_x = q_x' + q_x'' \tag{B5}$$

with $q_x' = -k\dfrac{dT}{dx}$, the Fourier heat-conduction law.

Wang Chang and Uhlenbeck (cited in ref. 15) give the currently accepted expressions for the Burnett stresses and heat flux, which reduce for one-dimensional flow to the following equations:

$$
\left.
\begin{aligned}
p_{xx}'' &= \left(\frac{2}{3}\omega_1 - \frac{14}{9}\omega_2 + \frac{8}{27}\omega_6\right)\frac{\mu^2}{p}\left(\frac{du}{dx}\right)^2 + \frac{2}{3}\frac{\mu^2}{\rho T}\omega_3\frac{d^2T}{dx^2} + \frac{2}{3}\omega_4\frac{\mu^2}{p\rho T}\frac{dp}{dx}\frac{dT}{dx} + \\
&\quad \frac{2}{3}\omega_5\frac{\mu^2}{\rho T^2}\left(\frac{dT}{dx}\right)^2 - \frac{2}{3}\frac{\mu^2}{\rho p}\omega_2\frac{d^2p}{dx^2} + \frac{2}{3}\frac{\mu^2}{\rho^2 p}\omega_2\frac{dp}{dx}\frac{d\rho}{dx} \\[2em]
q_x'' &= \frac{\mu^2}{\rho T}\left(\theta_1 + \frac{8}{3}\theta_2 + \frac{2}{3}\theta_3 + \frac{2}{3}\theta_5\right)\frac{du}{dx}\frac{dT}{dx} + \frac{2}{3}\frac{\mu^2}{\rho}\left(\theta_2 + \theta_4\right)\frac{d^2u}{dx^2} - \\
&\quad \frac{2}{3}\theta_3\frac{\mu^2}{\rho u}\left(\frac{du}{dx}\right)^2
\end{aligned}
\right\} \tag{B6}
$$

The values of the constants θ_i and ω_i are, for Maxwellian molecules

$$\omega_1 = 10/3 \qquad\qquad \theta_1 = 75/8$$

$$\omega_2 = 2 \qquad\qquad\qquad \theta_2 = -45/8$$

$$\omega_3 = 3 \qquad\qquad\qquad \theta_3 = -3$$

$$\omega_4 = 0 \qquad\qquad\qquad \theta_4 = 3$$

$$\omega_5 = 3 \qquad\qquad\qquad \theta_5 = 117/4$$

$$\omega_6 = 8$$

These numbers are now introduced, and the continuity equation and equation of state are used to eliminate the pressure and density variables. This gives the following set of six equations for six unknowns:

$$mu + \frac{mRT}{u} + p_{xx}' + p_{xx}'' = P$$

$$mu^2 + 5mRT + 2u(p_{xx}' + p_{xx}'') + 2(q_x' + q_x'') = Q$$

$$p_{xx}' = -\frac{4}{3}\mu\frac{du}{dx}$$

$$q_x' = -k\frac{dT}{dx}$$

$$p_{xx}'' = \frac{40}{27}\frac{\mu^2}{mRT}u\left(\frac{du}{dx}\right)^2 - \frac{4}{3}\frac{\mu^2}{mu}\left(\frac{du}{dx}\right)^2 + \frac{4}{3}\frac{\mu^2}{m}\frac{d^2u}{dx^2} + \frac{4}{3}\frac{\mu^2}{mT}\frac{du}{dx}\frac{dT}{dx} +$$

$$\frac{2}{3}\frac{\mu^2}{m}\frac{u}{T}\frac{d^2T}{dx^2} + 2\frac{\mu^2}{mT^2}u\left(\frac{dT}{dx}\right)^2$$

$$q_x'' = \frac{95}{8}\frac{\mu^2}{m}\frac{u}{T}\frac{du}{dx}\frac{dT}{dx} - \frac{7}{4}\frac{\mu^2}{m}u\frac{d^2u}{dx^2} + 2\frac{\mu^2}{m}\left(\frac{du}{dx}\right)^2$$

(B7)

The dimensionless variables suggested by Zoller are

$$v = \frac{mu}{P}$$

$$\tau = \frac{m\sqrt{2RT}}{P}$$

$$\eta' = \frac{p_{xx}'}{p} = \frac{up_{xx}'}{mRT}$$

$$\eta'' = \frac{p_{xx}''}{p} = \frac{up_{xx}''}{mRT}$$

$$\xi' = -\frac{4}{5}\frac{q_x'}{mRT}\frac{u}{\sqrt{2RT}}$$

$$\xi'' = -\frac{4}{5}\frac{q_x''}{mRT}\frac{u}{\sqrt{2RT}}$$

$$z = \frac{3}{8}\tau^2\frac{m}{\mu}x$$

$$a = \frac{mQ}{P^2}$$

(B8)

In these variables, the system of equations (B7) becomes

$$2v^2 - 2v + \tau^2(1 + \eta' + \eta'') = 0$$

$$v^2 + \tau^2\left[\frac{5}{2} + \eta' + \eta'' - \frac{5}{4}\frac{\tau}{v}(\xi' + \xi'')\right] = a$$

$$\eta' = -v\frac{dv}{dz}$$

$$\xi' = \frac{9}{4}v\frac{d\tau}{dz}$$

$$\eta'' = -\frac{3}{8}\tau^2\frac{d\eta'}{dz} + \frac{1}{6}\tau v\frac{d\xi'}{dz} + \left(\frac{5}{6} - \frac{3}{4}\frac{\tau^2}{v^2}\right)(\eta')^2 + \frac{14}{27}(\xi')^2 - \frac{1}{6}\frac{\tau}{v}\eta'\xi'$$

$$\xi'' = -\frac{63}{160}\tau v\frac{d\eta'}{dz} - \frac{27}{32}\frac{\tau}{v}(\eta')^2 + \frac{19}{8}\eta'\xi'$$

(B9)

The fourth of these equations involves the assumption that the Prandtl number is 2/3, which is satisfied exactly by Maxwell molecules and is nearly true for all pure monatomic gases.

If in equations (B9) the first two members are used to eliminate η'' and ξ'' from the last two members, a little rearranging of terms then leads to the following set of four first-order, nonlinear, ordinary differential equations

$$\frac{dv}{dz} = -\frac{\eta'}{v}$$

$$\frac{d\tau}{dz} = \frac{4}{9}\frac{\xi'}{v}$$

$$\frac{d\eta'}{dz} = -\frac{160}{63\tau v}R_2$$

$$\frac{d\xi'}{dz} = \frac{6}{\tau v}R_1 - \frac{40}{7v^2}R_2$$

(B10)

in which

$$R_1 = \frac{2v - 2v^2}{\tau^2} - 1 - \eta' + \left(\frac{3}{4}\frac{\tau^2}{v^2} - \frac{5}{6}\right)(\eta')^2 + \frac{1}{6}\frac{\tau}{v}\eta'\xi' - \frac{14}{27}(\xi')^2$$

$$R_2 = \frac{2v}{5\tau^3}\left[3(\tau^2 - \tau_\nu^2) + 4(v - v_\nu) - 2(v^2 - v_\nu^2)\right] - \xi' - \frac{19}{8}\xi'\eta' + \frac{27}{32}\frac{\tau}{v}(\eta')^2$$

$$\left.\begin{matrix}\\\\\\\\\end{matrix}\right\} \quad \text{(B11)}$$

The quantities τ_ν and v_ν, which appear in R_2, are the boundary values of τ and v far upstream or far downstream of the shock, that is, at $z = \mp\infty$. At these locations the stress and heat flux are presumed to vanish, so that the first two members of equation (B9) can be quickly solved for τ_ν and v_ν in terms of a, the shock strength parameter. This gives first

$$2v_\nu^2 - 2v_\nu + \tau_\nu^2 = 0$$

$$v_\nu^2 + \frac{5}{2}\tau_\nu^2 = a$$

$$\left.\begin{matrix}\\\\\\\end{matrix}\right\} \quad \text{(B12)}$$

The index ν will be given the value 0 to indicate conditions far upstream of the shock $(z = -\infty)$, and $\nu = 1$ to indicate downstream conditions.

Since the boundary conditions are specified at the singular points of equations (B10), a special investigation of the solutions in the vicinity of these points is a prerequisite for numerical integration. For this purpose one sets

$$v = v_\nu + \Omega$$

$$\tau = \tau_\nu - \vartheta$$

$$\eta' = \eta'$$

$$\xi' = \xi'$$

$$\left.\begin{matrix}\\\\\\\\\\\\\end{matrix}\right\} \quad \text{(B13)}$$

where Ω, ϑ, η', and ξ' are quantities negligible to any order higher than the first in the vicinity of the singular point. Next one assumes

$$\left.\begin{array}{l} \Omega = \bar{\Omega}e^{\lambda z} \\[8pt] \vartheta = \bar{\vartheta}e^{\lambda z} \\[8pt] \eta' = \bar{\eta}e^{\lambda z} \\[8pt] \xi' = \bar{\xi}e^{\lambda z} \end{array}\right\} \tag{B14}$$

Then there is obtained from equations (B10) the set of linear algebraic equations

$$\left.\begin{array}{l} \lambda\bar{\Omega} = -\dfrac{\bar{\eta}}{v_\nu} \\[14pt] \lambda\bar{\vartheta} = -\dfrac{4}{9}\dfrac{\bar{\xi}}{v_\nu} \\[14pt] \lambda\bar{\eta} = -\dfrac{160}{63\tau_\nu v_\nu}\left(\dfrac{4}{5}\dfrac{\bar{\Omega}}{\tau_\nu} - \dfrac{12}{5}\dfrac{v_\nu}{\tau_\nu{}^2}\bar{\vartheta} - \bar{\xi}\right) \\[20pt] \lambda\bar{\xi} = \dfrac{6}{\tau_\nu v_\nu}\left(\dfrac{2}{\tau_\nu}\bar{\vartheta} - \dfrac{2}{\tau_\nu{}^2}(2v_\nu - 1)\bar{\Omega} - \bar{\eta}\right) - \dfrac{40}{7v_\nu{}^2}\left(\dfrac{4}{5}\dfrac{\bar{\Omega}}{\tau_\nu} - \dfrac{12}{5}\dfrac{v_\nu}{\tau_\nu{}^2}\bar{\vartheta} - \bar{\xi}\right) \end{array}\right\} \tag{B15}$$

which has nonzero solutions only if λ satisfies the characteristic equation

$$189v_\nu{}^6(1 - v_\nu)^3\lambda^4 - 1080v_\nu{}^4(1 - v_\nu)^3\lambda^3 + 2328v_\nu{}^3(1 - v_\nu)^2\lambda^2 -$$

$$96v_\nu(1 - v_\nu)(38v_\nu - 15)\lambda + 256(8v_\nu - 5) = 0 \tag{B16}$$

From the four roots of this quartic, one which meets the requirements of physical reality can be selected for each value of ν. The requirements are that the real part of λ be positive for $\nu = 0(z = -\infty)$ and negative for $\nu = 1(z = \infty)$ and that $\lambda \to 0$ as $v_0 \to v_1 \to 5/8$ (that is, as the shock strength vanishes).

When λ is a root of equation (B16) the first three members of equations (B15) can be solved for the ratios $\overline{\vartheta}/\overline{\Omega}$, $\overline{\eta}/\overline{\Omega}$, and $\overline{\xi}/\overline{\Omega}$, yielding

$$
\left.
\begin{aligned}
\frac{\overline{\vartheta}}{\overline{\Omega}} &= \sqrt{2\left(\frac{1-v_\nu}{v_\nu}\right)\left(\frac{128 - 126v_\nu^3(1-v_\nu)\lambda^2}{384 - 720v_\nu(1-v_\nu)\lambda}\right)} \\[2mm]
\frac{\overline{\eta}}{\overline{\Omega}} &= -v_\nu\lambda \\[2mm]
\frac{\overline{\xi}}{\overline{\Omega}} &= -\frac{9}{4}v_\nu\lambda\frac{\overline{\vartheta}}{\overline{\Omega}}
\end{aligned}
\right\}
\qquad\qquad (B17)
$$

The initial values of v, τ, η, and ξ are then established for the purposes of computation by choosing the point $z = 0$ to correspond to some small but finite value of $\overline{\Omega}$. The initial derivatives at that point can then be found from equations (B10) or by differentiating equations (B14). The two methods will give nearly the same numbers if the starting value of $\overline{\Omega}$ is sufficiently small.

To insure the stability of machine integrations, one must determine by examination of the roots of equation (B16) whether to start near the upstream limit of the shock and integrate downstream or vice versa. The real parts of these roots are plotted versus v_ν in figure 10.

At $\nu = 1$ $(0.25 \leqq v_\nu \leqq 0.625)$ there are either four real roots, three positive and one negative, or two real roots of opposite sign plus a pair of complex conjugates with positive real part. The physically acceptable root is the negative real one. This singular point is of a saddle-point type and is ideal as a starting point for numerical integration.

At $\nu = 0$ $(0.625 \leqq v_\nu \leqq 1)$ the singular point has a variety of types, none of which are suitable for the initiation of numerical integration. These types dictate qualitatively the behavior of the numerical solution as it approaches its upstream limit. Thus, for $0.625 \lessapprox v_\nu \lessapprox 0.80$ the solution will come in monotonically, for $0.80 \lessapprox v_\nu \lessapprox 0.94$ a damped oscillatory approach can be expected, and for $0.94 \lessapprox v_\nu \leqq 1$ this oscillation may amplify rather than damp out. This behavior has been qualitatively confirmed by the computing machine, which also indicated that up

to Mach 2 the oscillations encountered are so small as to be barely noticeable.

Integrations were consequently started from downstream, with the arbitrary choice $\overline{\Omega}$ = 0.001, and proceeded toward increasingly negative values of z. They were performed on the NAREC digital computer of the Naval Research Laboratory, Washington, D. C. Numerical experiments confirmed that, with a Runge-Kutta third-order integration method (ref. 23) and integration steps equal to about 0.025 times the maximum-slope shock thickness, the results were independent of further reduction of step size to an accuracy considerably greater than that required here. The results also showed a high degree of independence of small variations in the initial derivative data, as would be expected of an integration starting out of a saddle point. These computations were programed and supervised by Mr. John L. Hammersmith of NRL, to whom the authors are greatly indebted.

To express these results in the nomenclature used elsewhere in this report, the molecular speed ratio $s = v/\tau$ and the following relations were necessary:

$$\frac{p_{xx}}{p} = \frac{2v - 2v^2}{\tau^2} - 1$$

$$\frac{q_x}{pu} = \frac{a - 2v + v^2}{\tau^2} - \frac{3}{2}$$

$$\epsilon = \sqrt{25 - 16a} \qquad \text{(Grad's shock-strength parameter)}$$

$$y = \frac{1024}{1575} \epsilon \left(1 - \frac{\epsilon^2}{25}\right)^{-1} z$$

$$\frac{\mu_*}{pu\delta_m(x)} = \frac{45}{256}\left(1 - \frac{\epsilon^2}{25}\right)\frac{1}{\delta_m(z)}$$

$$w = \frac{8v - 5}{\epsilon}$$

(B18)

REFERENCES

1. Sherman, F. S.: A Low-Density Wind-Tunnel Study of Shock-Wave Structure and Relaxation Phenomena in Gases. NACA TN 3298, 1955.

2. Maslach, G. J., and Sherman, F. S.: Design and Testing of an Axisymmetric Hypersonic Nozzle for a Low-Density Wind Tunnel. WADC TR-56-341, Aug. 1956.

3. Sherman, F. S.: New Experiments on Impact-Pressure Interpretation in Supersonic and Subsonic Rarefied Air Streams. NACA TN 2995, 1953.

4. D'yakov, S. P.: Shock Waves in Binary Mixtures. (In Russian.) Zhur. Eksp. Theoret. Fiz., vol. 27, no. 6, Dec. 1954, pp. 728-734.

5. Stalder, Jackson R., Goodwin, Glen, and Creager, Marcus O.: A Comparison of Theory and Experiment for High-Speed Free-Molecule Flow. NACA Rep. 1032, 1951. (Supersedes NACA TN 2244.)

6. Grad, H.: The Profile of a Steady Plane Shock Wave. Com. Pure and Appl. Math., vol. V, no. 3, Aug. 1952, pp. 257-300.

7. Chapman, Sydney, and Cowling, T. G.: The Mathematical Theory of Non-Uniform Gases. The Univ. Press (Cambridge), 1939.

8. Grad, H.: On the Kinetic Theory of Rarefied Gases. Com. Pure and Appl. Math., vol. II, no. 4, Dec. 1949, pp. 331-407.

9. Gilbarg, D., and Paolucci, D.: The Structure of Shock Waves in the Continuum Theory of Fluids. Jour. Rational Mech. and Analysis, vol. 2, no. 4, 1953, pp. 617-642.

10. Zoller, K.: Zur Struktur des Verdichtungsstosses. Zs. Phys., Bd. 130, Heft 1, 1951, pp. 1-38.

11. Bell, S., and Schaaf, S. A.: Heat Transfer to a Cylinder for the Free Molecule Flow of a Nonuniform Gas. Jet Propulsion, vol. 25, no. 4, Apr. 1955, pp. 168-169.

12. Ikenberry, E., and Truesdell, C.: On the Pressures and the Flux of Energy in a Gas According to Maxwell's Kinetic Theory, I. Jour. Rational Mech. and Analysis, vol. 5, no. 1, Jan. 1956, pp. 1-54.

13. Truesdell, C.: On the Pressures and the Flux of Energy in a Gas According to Maxwell's Kinetic Theory, II. Jour. Rational Mech. and Analysis, vol. 5, no. 1, Jan. 1956, pp. 55-128.

14. Bromley, L. A., and Wilke, C. R.: Viscosity Behavior of Gases.
    Ind. and Eng. Chem., vol. 43, no. 7, July 1951, pp. 1641-1648.

15. Lin, T. C., and Street, R. E.: Effect of Variable Viscosity and
    Thermal Conductivity on High-Speed Slip Flow Between Concentric
    Cylinders. NACA Rep. 1175, 1954. (Supersedes NACA TN 2895.)

16. Wang Chang, C. S.: On the Theory of Thickness of Weak Shock Waves.
    CM-503, Appl. Phys. Lab., The Johns Hopkins Univ., Aug. 1948.

17. Broer, L. J. F.: On the Theory of Shock Structure I. Appl. Sci.
    Res., vol. A3, no. 5, 1952, pp. 349-360.

18. Schaaf, S. A.: Theoretical Considerations in Rarefied Gas Dynamics.
    Ch. IX, Symposium on Heat Transfer, Univ. of Mich. Press (Ann
    Arbor), 1953, pp. 237-260.

19. Sherman, F. S.: Transport Phenomena in Low-Density Gases. Ch. XV,
    Transport Properties in Gases, Northwestern Univ. Press (Evanston),
    1958, pp. 134-142.

20. Hornig, D. F.: Energy Exchange in Shock Waves. Jour. Phys. Chem.,
    vol. 61, July 1957, pp. 856-860.

21. Snyder, N. W.: Radiation in Metals. Trans. ASME, vol. 76, no. 4,
    May 1954, pp. 541-548.

22. Devienne, M.: Conduction Termique dans les gaz rarefies. Coefficient
    d'accomodation. Memorial des sciences physiques, Acad. Sci.,
    fasc. LVI, Gauthier-Villars (Paris), 1953.

23. Hildebrand F. B.: Introduction to Numerical Analysis. McGraw-Hill
    Book Co., Inc., 1956.

TABLE I.- SUMMARY OF FLOW PROPERTIES

$$\left[T_o = 296.5° \text{ K}; \quad R = 2.086 \times 10^6 \text{ erg/°K}; \quad \mu_* = 1.763 \times 10^{-4} \text{ poise} \right]$$

M_1	ϵ	ρu, gm/cm² sec	L_*, cm	L_1, cm	Λ_1, cm	y/x, cm⁻¹	$\delta_m^{(u)}$, cm (a)	$\dfrac{\Lambda_1}{\delta_m^{(u)}}$	$\dfrac{L_*}{\delta_m^{(u)}}$
1.335	0.985	0.00758	0.0233	0.0198	0.0425	4.84	0.416	0.104	0.056
1.454	1.232	.00846	.0208	.0166	.0399	6.75	.294	.134	.071
1.576	1.444	.00940	.0188	.0140	.0365	8.80	.230	.160	.082
1.713	1.642	.01020	.0173	.0120	.0338	10.86	.188	.180	.092

[a]Equivalent velocity thicknesses, obtained from measured wire-temperature thicknesses by use of equation (9).
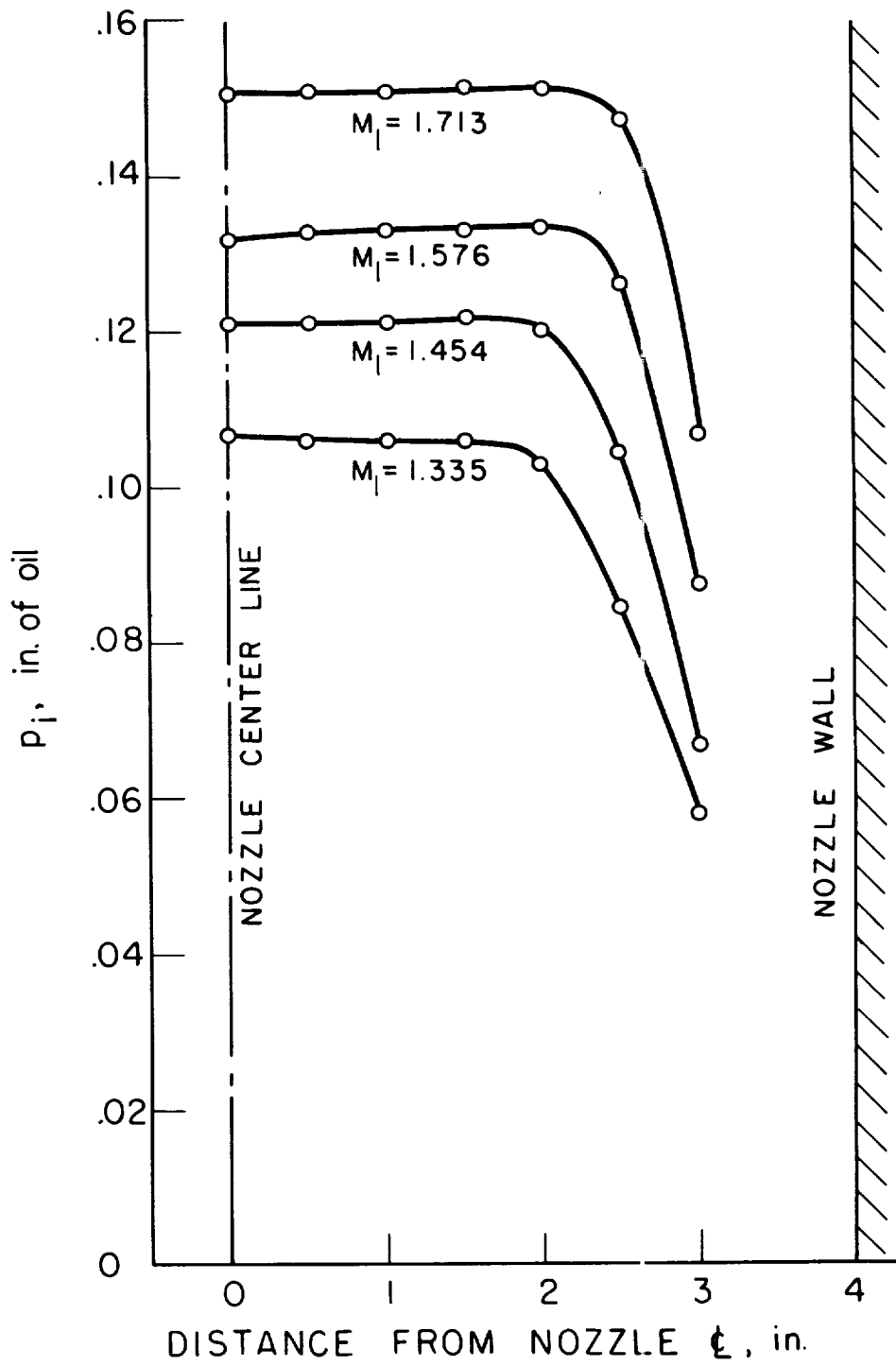
Figure 1.- Impact pressure surveys; Mach 1.5 nozzle.
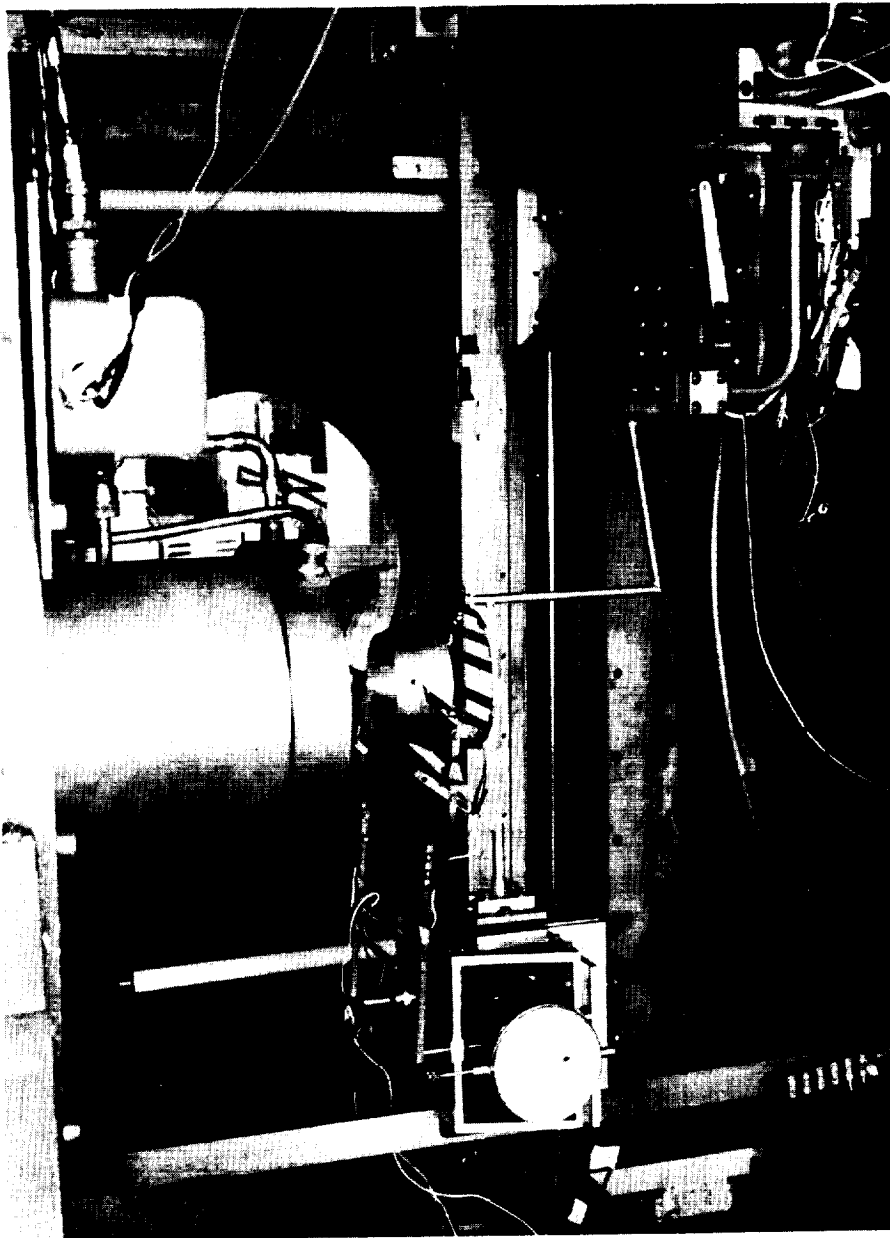
L-58-943a

Figure 2.- Shock holder and wire-traverse mechanism.

40

L-58-944a
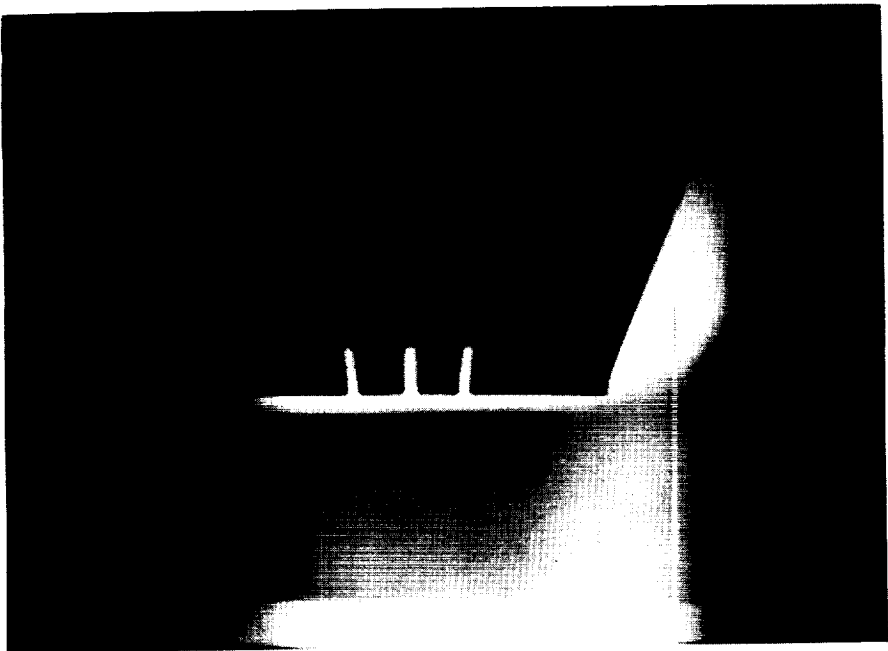
(a) Shock wave at $M_1 = 1.335.$ (b) Shock wave at $M_1 = 1.713.$

Figure 3.- Glow photographs of shock-holder operation.

12-14-58W

SHOCK-HOLDER
ENTRY

CURRENT
LEAD

POTENTIAL
LEAD

COPPER-PLATED
LAP JOINT

0.00025" DIAM.
TUNGSTEN
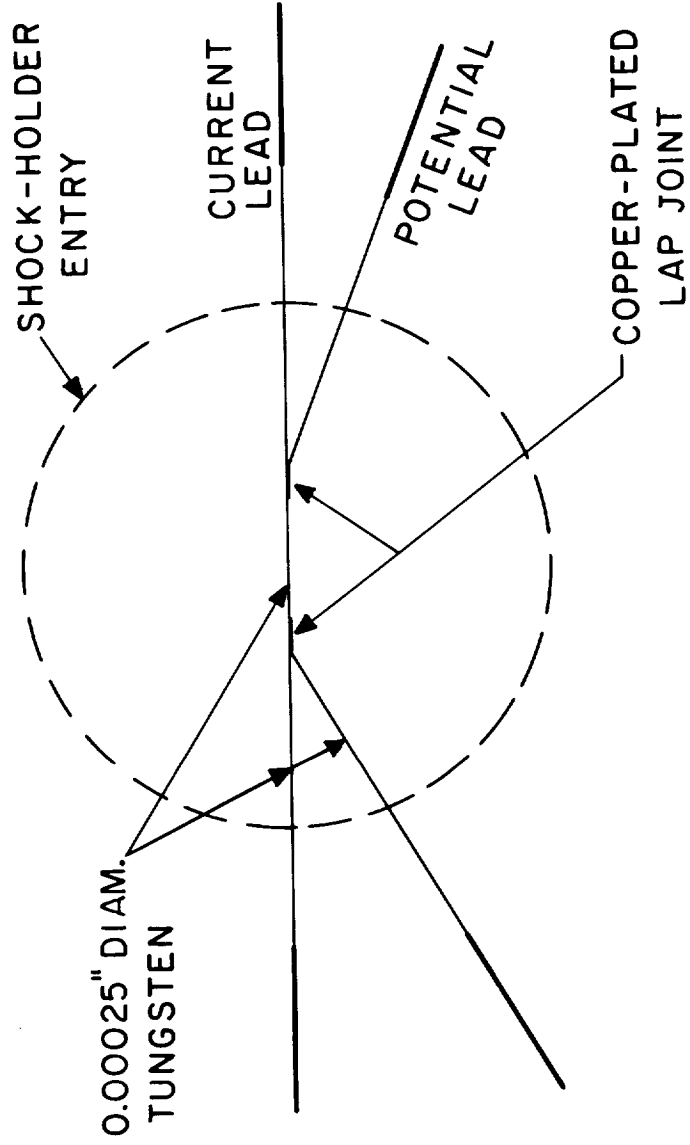
Figure 4.- Schematic diagram of resistance-wire probe.
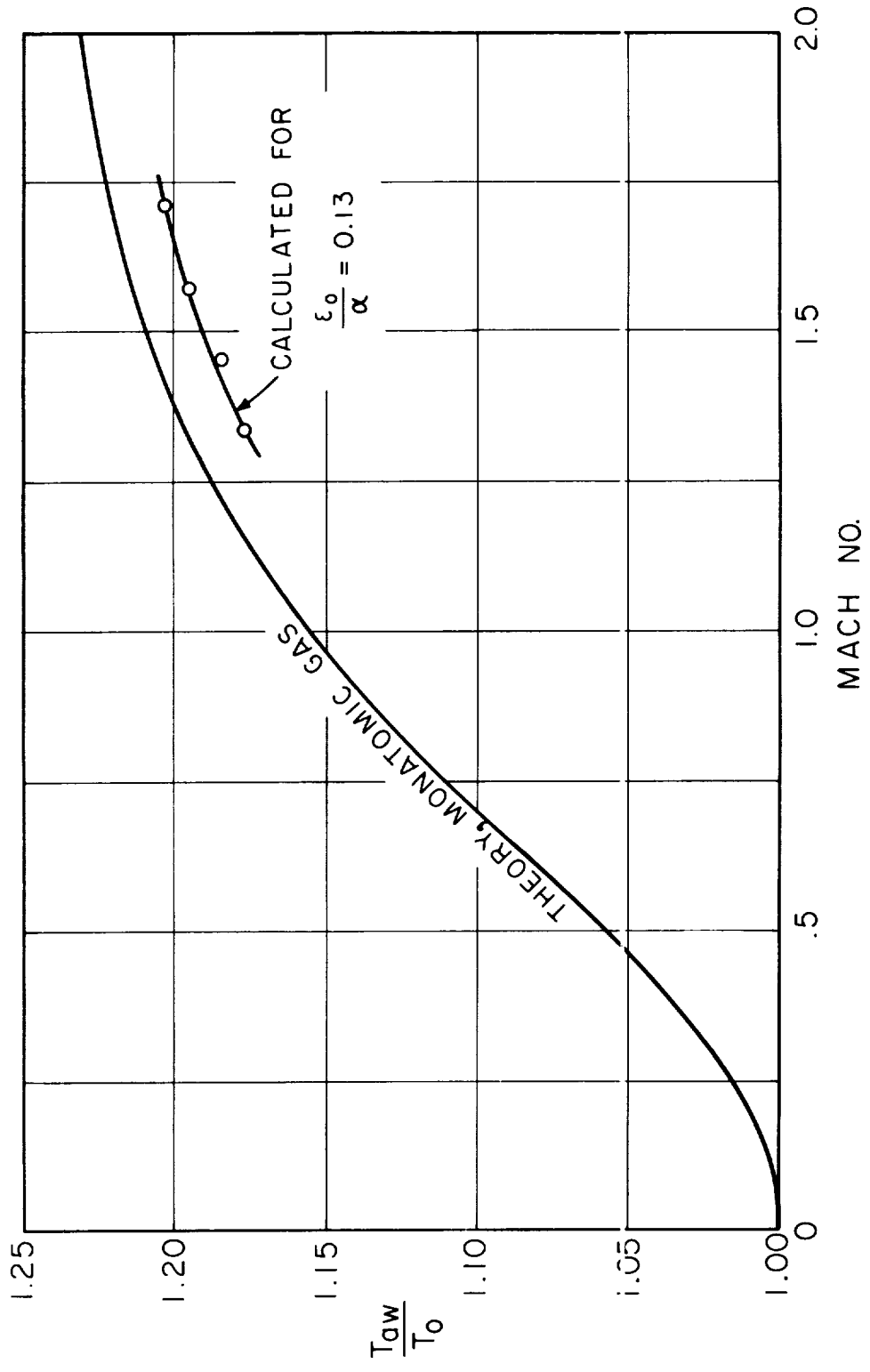
Figure 5.- Comparison of experiment and theory (ref. 4) for probe temperature in uniform stream.
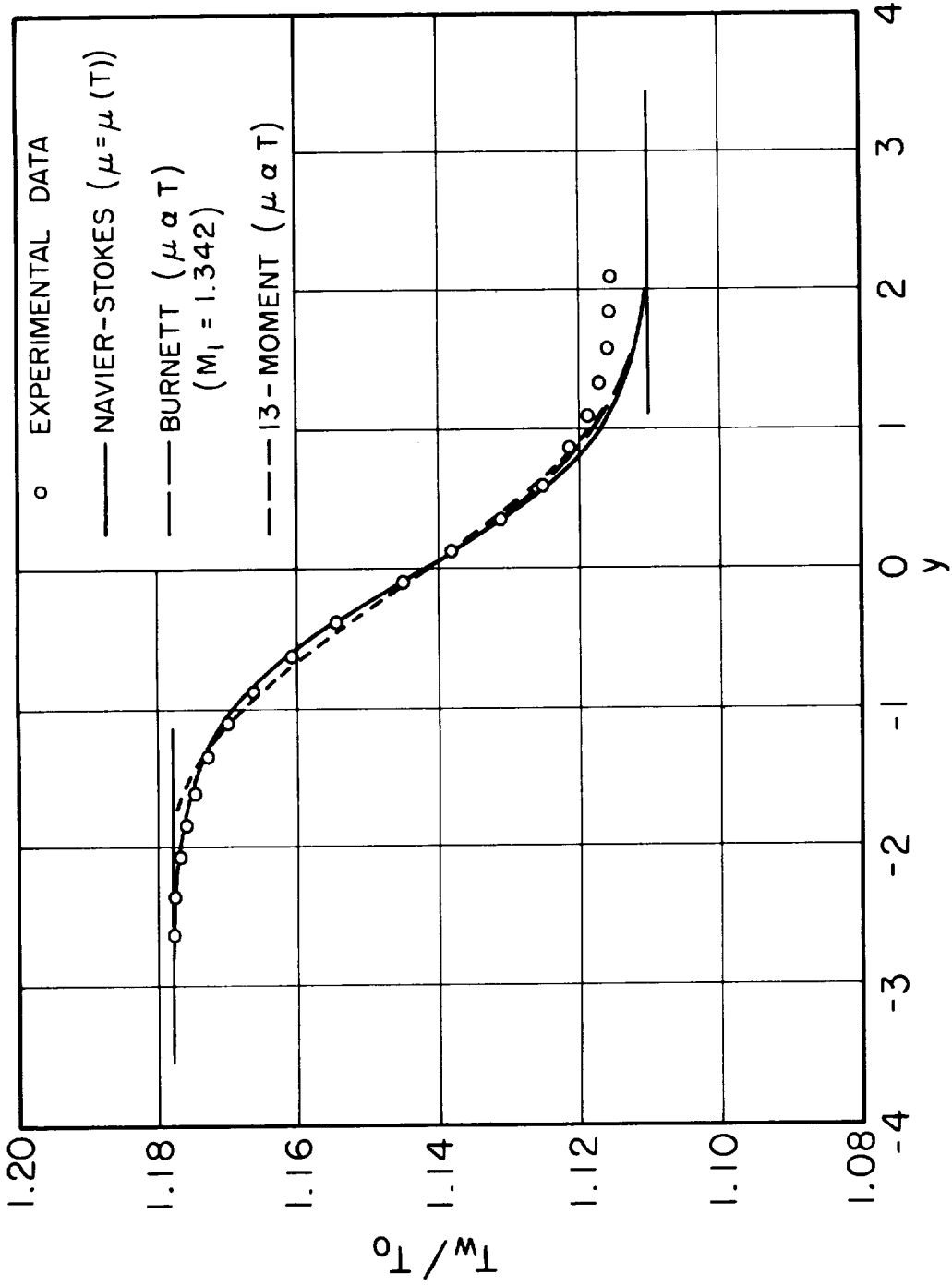
12-14-58W

(a) $M_1 = 1.335$.

Figure 6.- Temperature profiles.
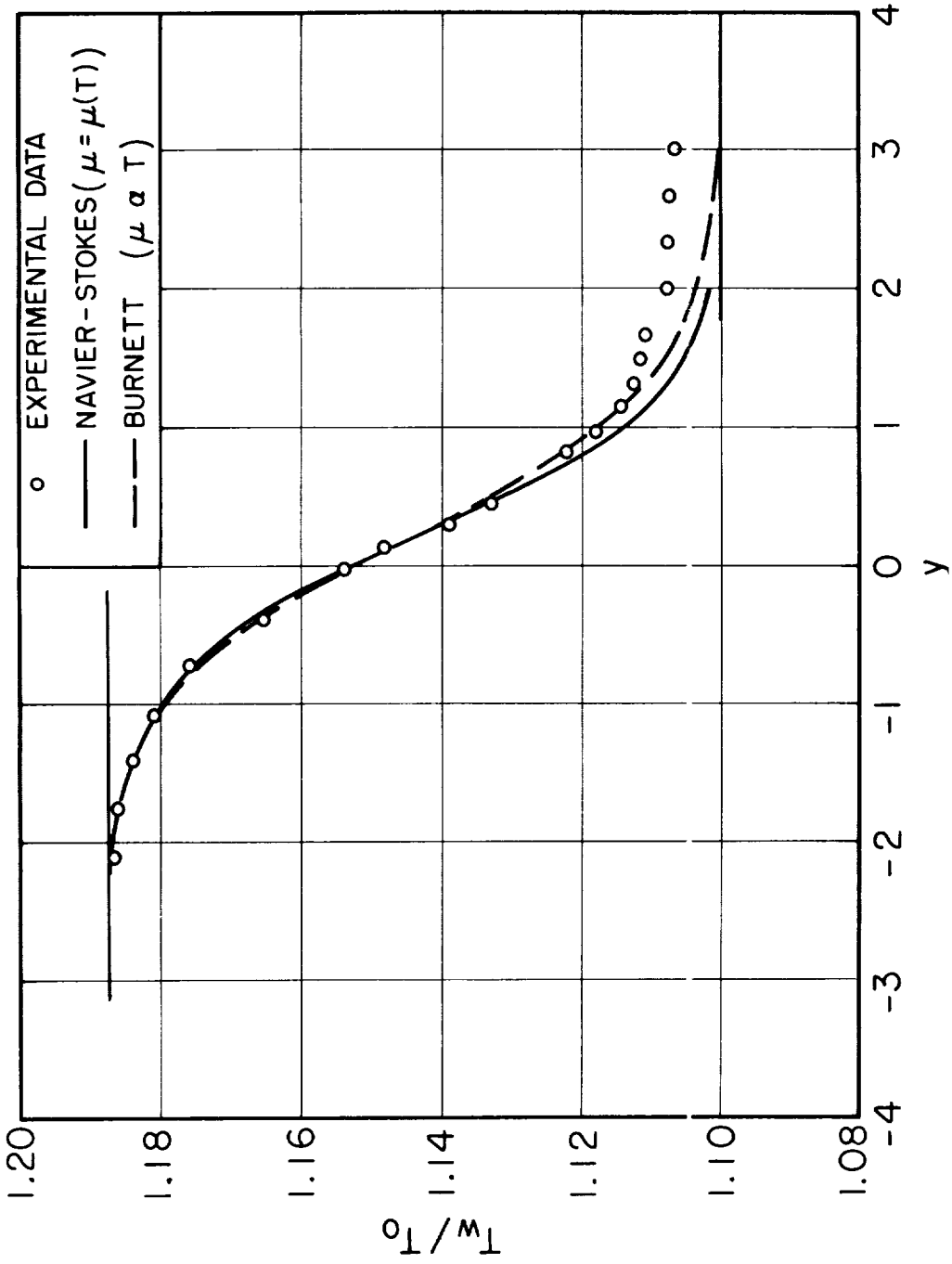
(b) $M_1 = 1.454$.

Figure 6.- Continued.
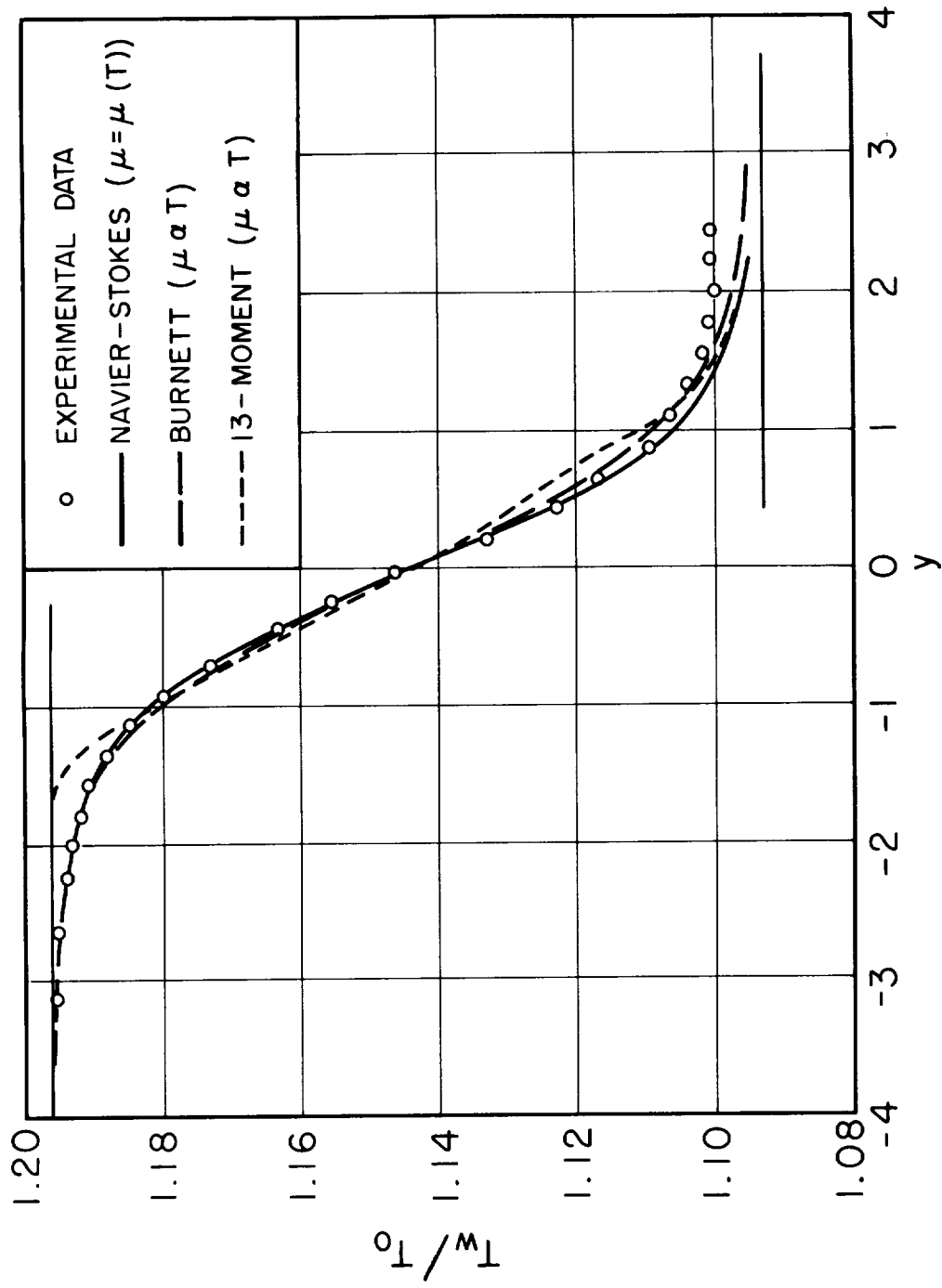
(c) $M_1 = 1.576$.

Figure 6.- Continued.
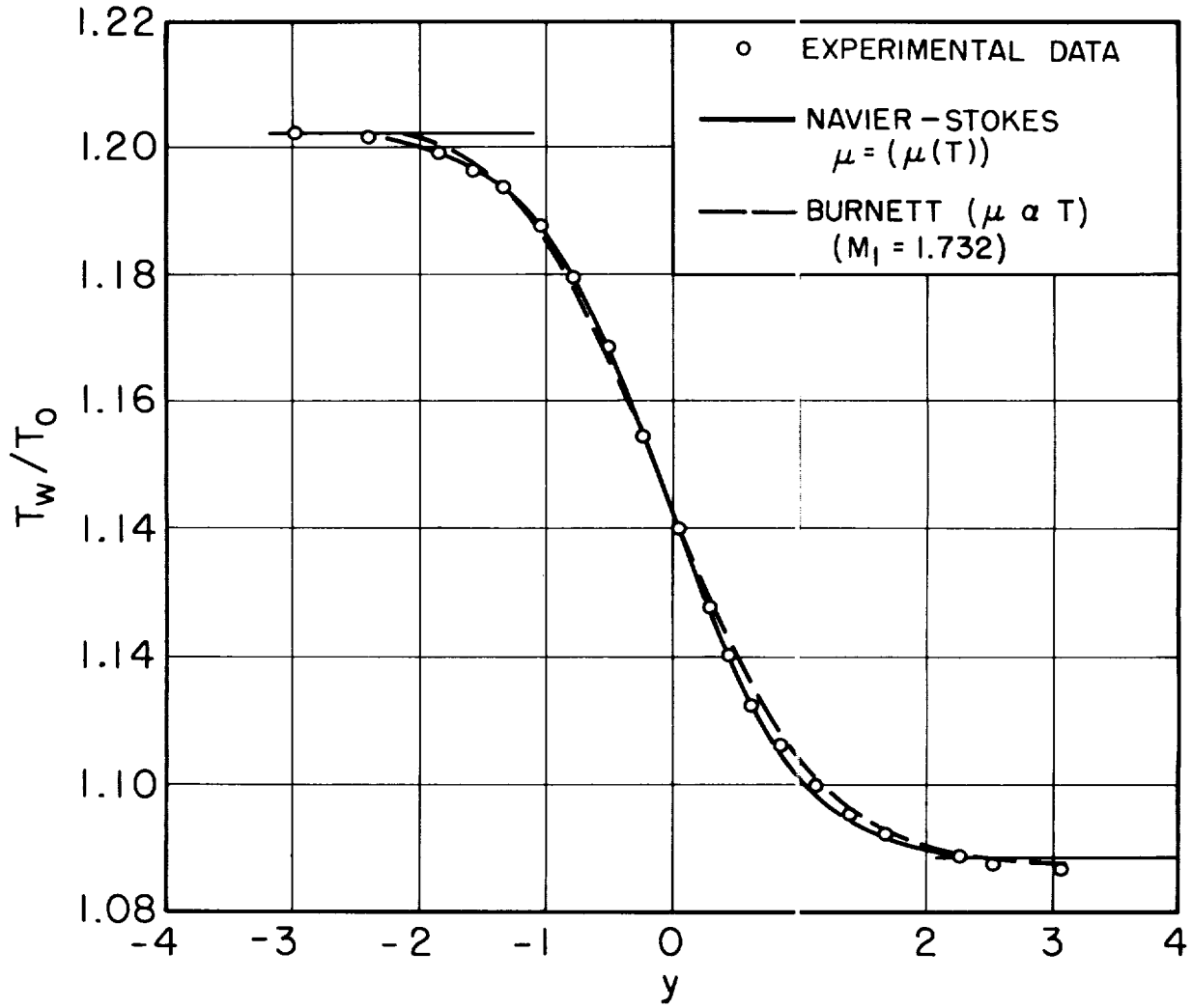
(d) $M_1 = 1.713$.

Figure 6.- Concluded.
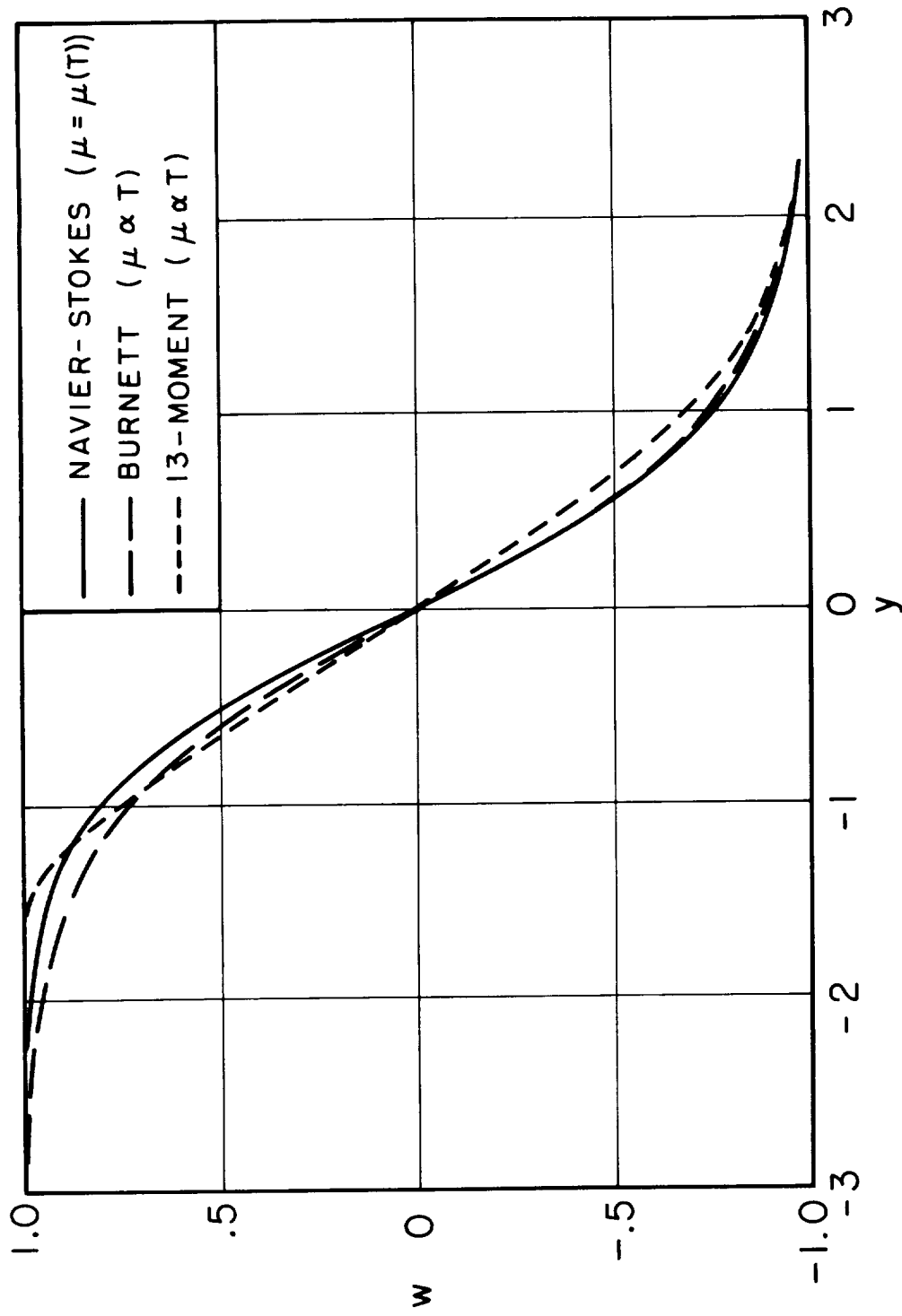
(a) $M_1 = 1.576.$

Figure 7.- Velocity profiles.
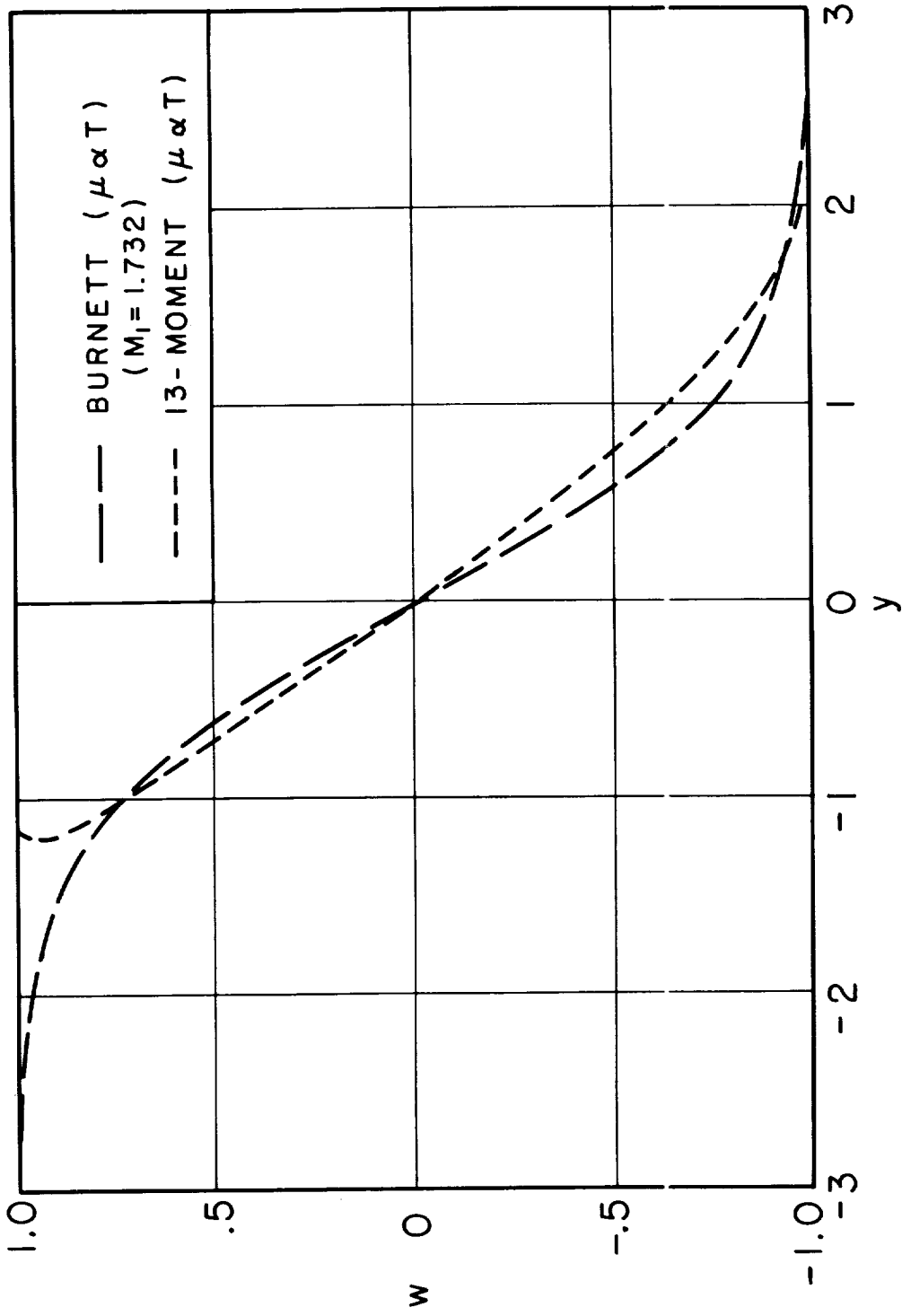
(b) $M_1 = 1.713$.

Figure 7.- Concluded.

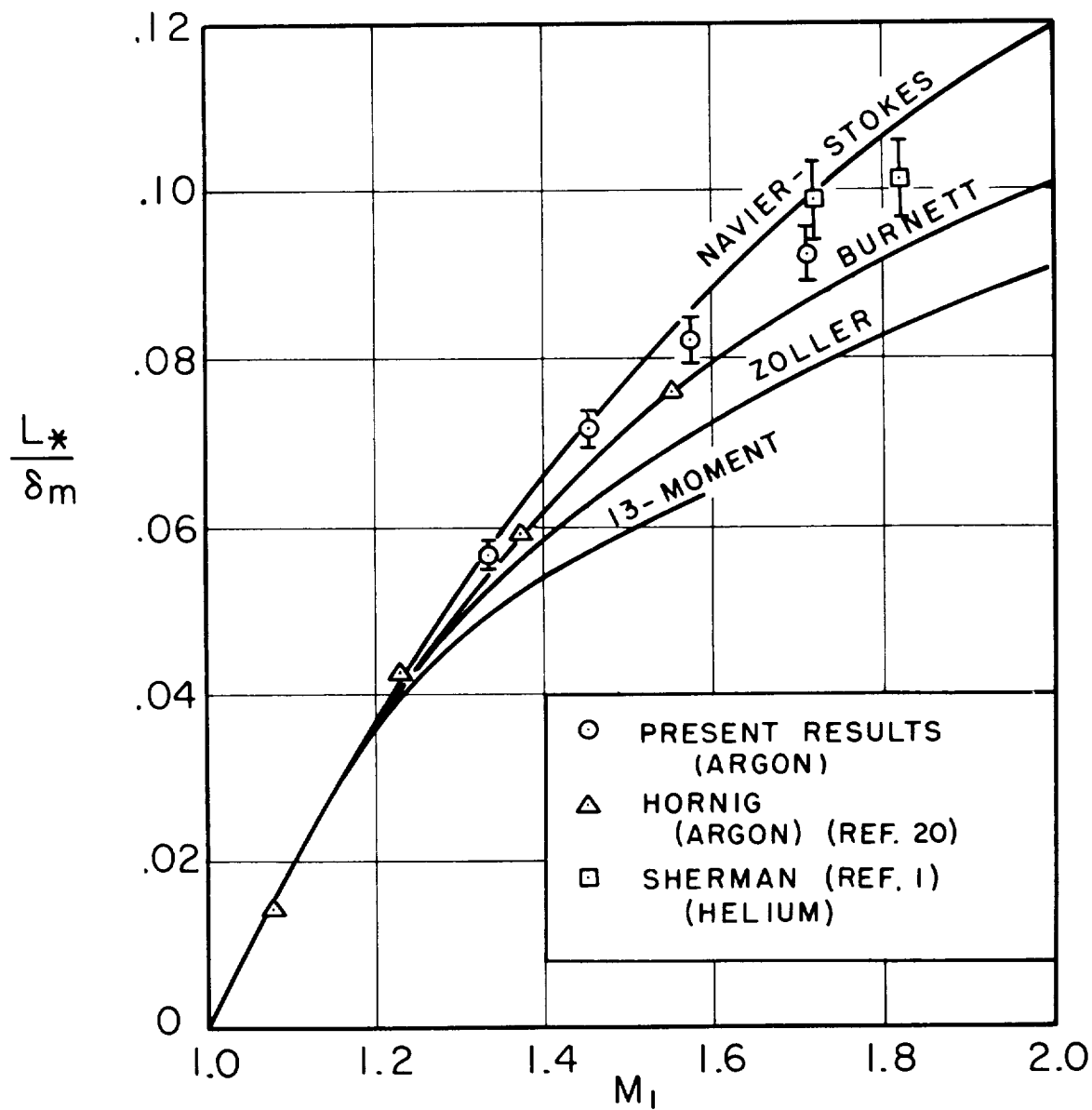12-14-58W

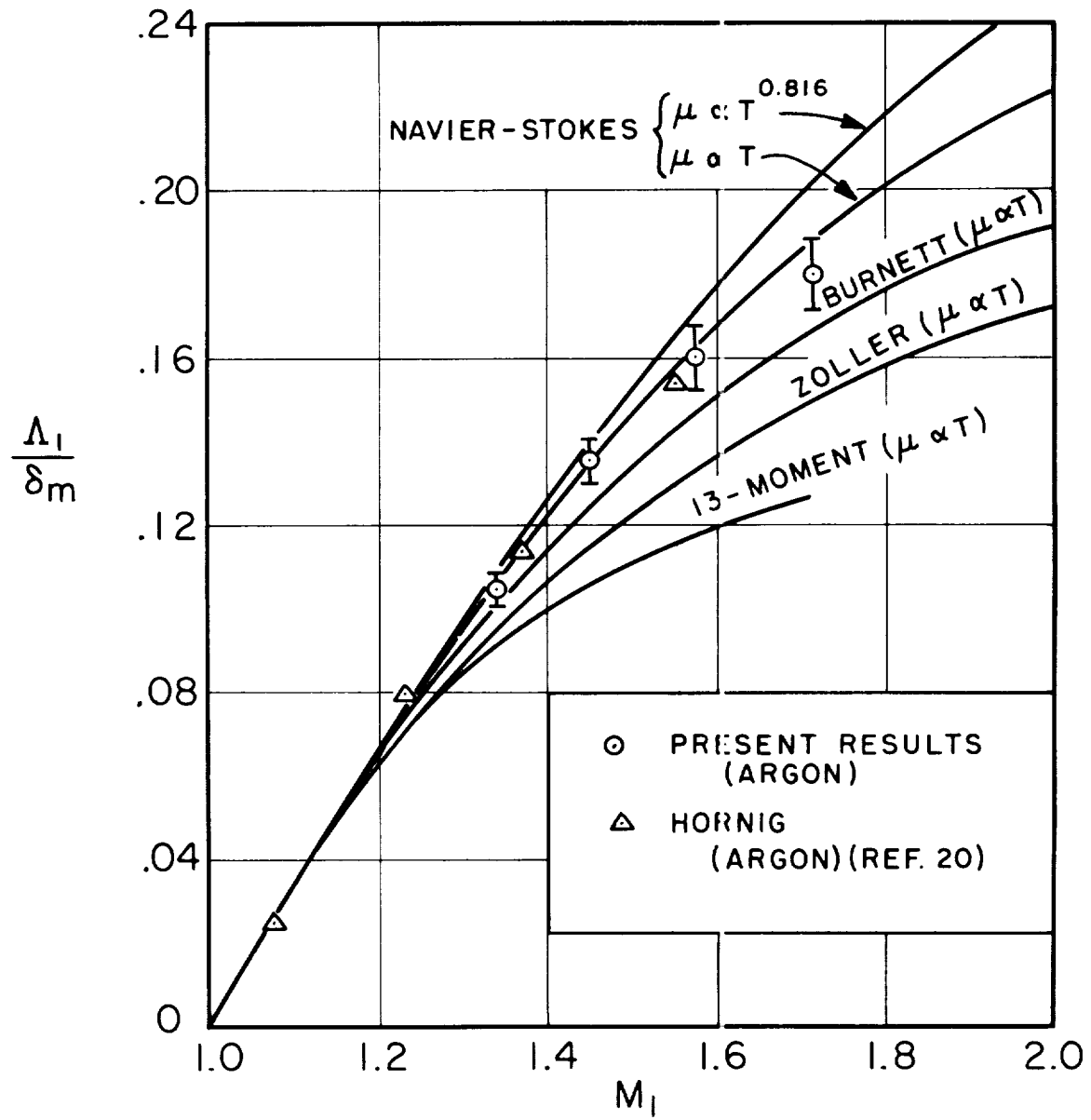Figure 8.- Shock-wave thickness in terms of reference length L_*.
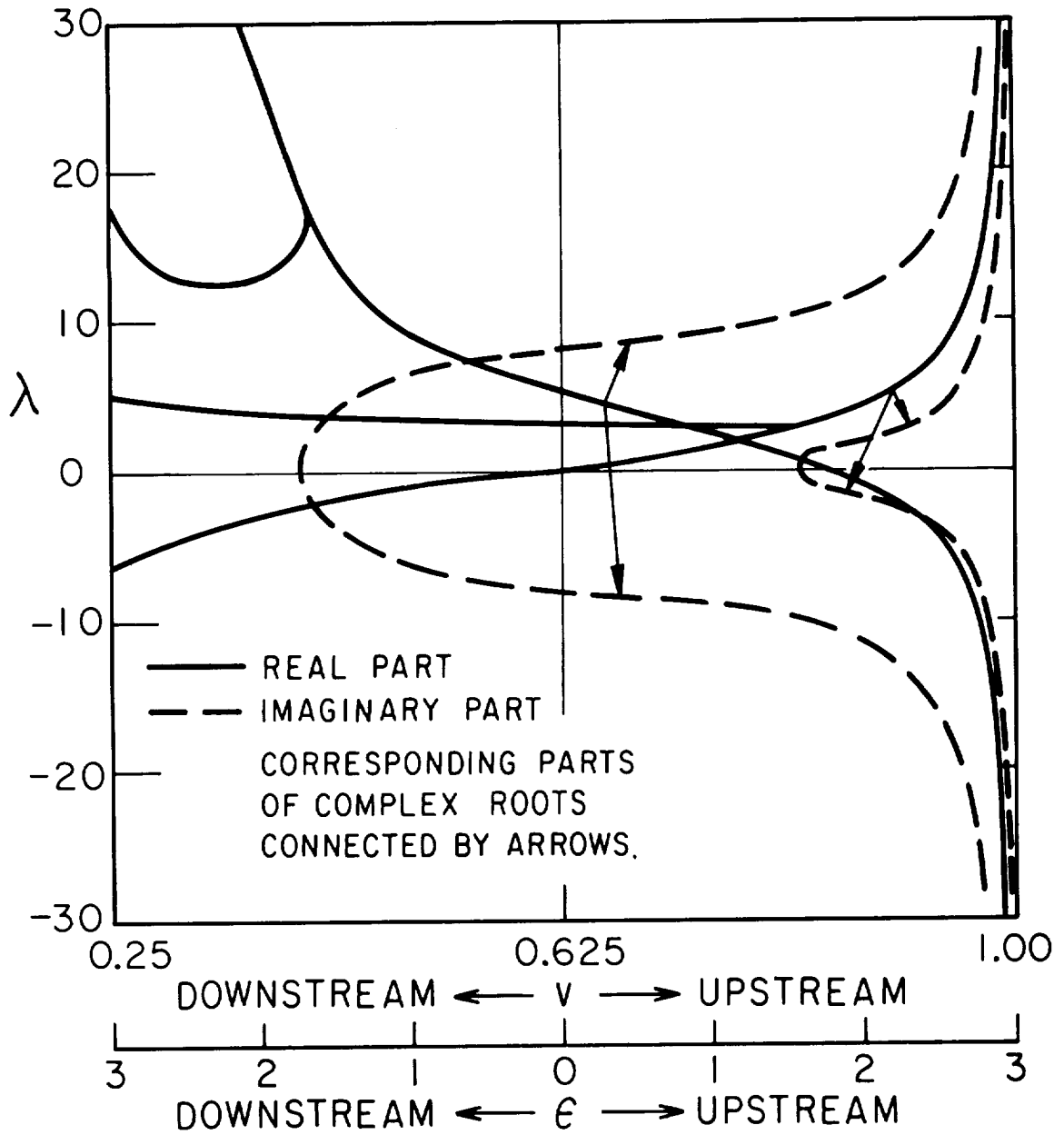
Figure 9.- Shock-wave thickness in terms of upstream mean free path.

Figure 10.- Roots of equation (B16).